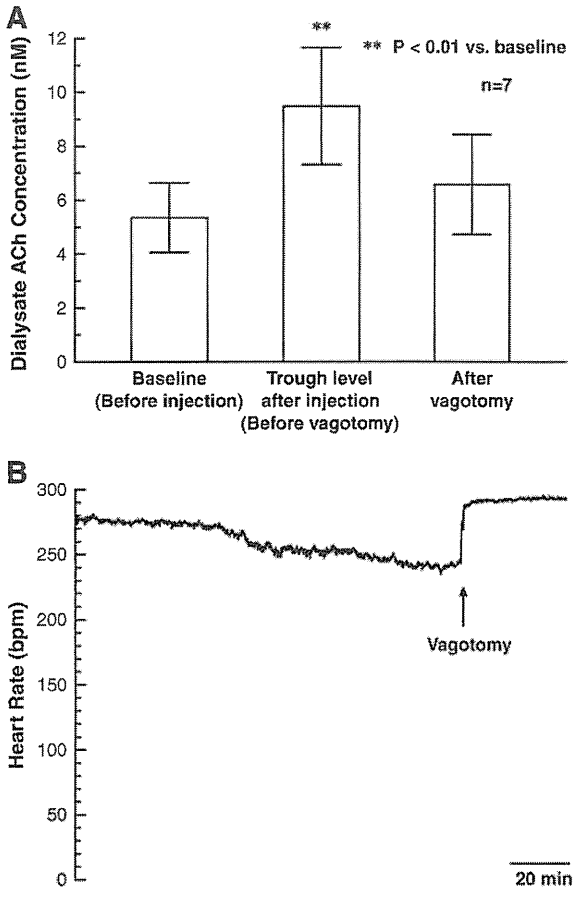

Fig. 3. A: Effect of vagotomy after icv injection of 1 nmol of ghrelin on dialysate ACh concentration (n = 7). Values are mean ± SE. Statistical comparison was performed after logarithmic transformation. ** P<0.01 vs. baseline before injection by one-way repeated measures analysis of variance followed by Dunnett's test. B: Typical time course of heart rate change. Heart rate gradually decreased after icv injection of ghrelin and promptly returned to the baseline level after vagatomy.

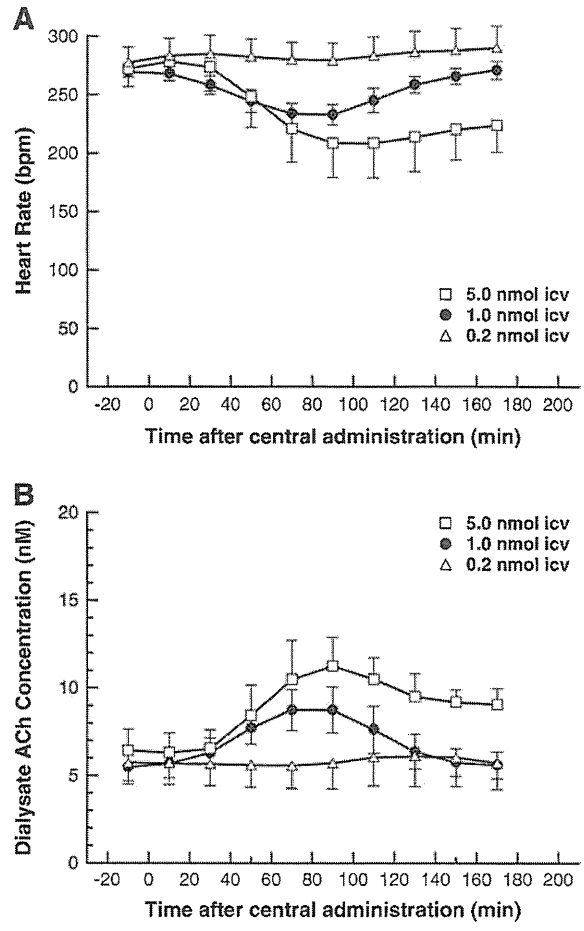

Fig. 4. Time courses of heart rate (A) and dialysate ACh concentration (B) elicited by icv injection of 0.2 nmol (△, n = 3) or 5 nmol (□, n = 4) of ghrelin. Graphs of icv injection of 1 nmol of ghrelin (●) were reproduced from Figs. 1A and 2A for intuitive comparison.

demonstrated that icv injection of ghrelin stimulates pancreatic secretion by activating efferent vagal nerves. Kobashi et al. (2009) have shown that icv injection of ghrelin induces relaxation of the proximal stomach through activation of efferent vagal nerves. Vagal nerves also play an important role in the regulation of heart rate under physiological conditions. Moreover, vagal stimulation has cardioprotective effect against chronic heart failure (Li et al., 2004; Schwartz et al., 2008). However, the effect of icv injection of ghrelin on cardiac vagal nerve activity has not been reported.

In the present study, icv injection of ghrelin decreased heart rate without affecting mean arterial pressure, and simultaneously increased dialysate ACh concentration without changing dialysate NE concentration. The time course of heart rate changes parallels that of dialysate ACh concentration changes throughout the experiment. Furthermore, dialysate ACh concentration and heart rate recovered to the baseline levels immediately after vagotomy. Thus, the decrease in heart rate by central ghrelin could be due to cardiac vagal activation and not cardiac sympathetic suppression. The present study demonstrates that centrally administered ghrelin activates cardiac vagal nerve and decreases heart rate. The maximal dialysate ACh concentration following icv injection of ghrelin reached 8.8 ± 1.2 nM. This dialysate ACh concentration is almost equivalent to that induced by electrical stimulation of the right cervical vagal nerve at 10–20 Hz (Shimizu et al., 2009). Therefore, ghrelin may be one of the most important mediators in the central nerve system, which activates cardiac vagal nerve.

Ghrelin receptors are present in the central nerve system. In a c-Fos expression study, Date et al. (2001) reported that central ghrelin activated the NTS and dorsal motor nucleus of the vagus (DMNV). Zigman et al. (2006) demonstrated the presence of GHS-R in all three divisions of the dorsal vagal complex using in situ hybridization. The GHS-Rs are also expressed in the hypothalamus including the ARC (Guan et al., 1997). Central administration of ghrelin may activate cardiac vagal nerve through direct action on central ghrelin receptors, although it is difficult to determine the brain region in which ghrelin acts from the present study.

There was a long time lag between icv injection of ghrelin and activation of the cardiac vagal nerve. This may suggest that other mediators are involved in ghrelin-induced activation of cardiac vagal nerve. Intracerebroventricular injection of ghrelin evokes growth hormone release (Date et al., 2000). Resmini et al. (2006) reported sympathovagal imbalance due to vagal hypertone in acromegalic patients. Sato et al. (2003), however, suggested that the stimulatory effect of ghrelin on pancreatic secretion may be induced independent of its growth-hormone releasing effect, because a maximal increase in growth hormone was observed 10–20 min after ghrelin injection but a peak increase in pancreatic secretion was found 30–60 min after injection. In the present study, the maximal decrease in heart rate (234 ± 9 and 233 ± 9 bpm) and maximal increase in dialysate ACh concentration (8.8 ± 1.2 and 8.7 ± 1.3 nM) were both observed during 60–100 min after icv ghrelin injection. Moreover, Bisi et al. (1999) reported that intravenous administration of recombinant human growth hormone increased circulating growth hormone levels but did

not affect heart rate or mean arterial pressure in humans. Therefore, the stimulatory effect of ghrelin on the cardiac vagal nerve may be independent of its growth hormone releasing effect.

Nakazato et al. (2001) reported that antibodies and antagonists of neuropeptide Y and agouti-related protein abolished ghrelin-enhanced feeding. Kamegai et al. (2001) reported that chronic icv infusion of ghrelin increased both neuropeptide Y and agouti-related protein mRNA levels in the ARC. Moreover, Kobashi et al. (2006) showed that central neuropeptide Y induced proximal stomach relaxation via Y1 receptors in the dorsal vagal complex of rats. Thus, neuropeptide Y and agouti-related protein may be involved in the stimulatory effect of ghrelin on cardiac vagal nerve. However, we need further investigations to identify the mediators involved in the ghrelin-induced cardiac vagal activation.

4.2. Ghrelin and cardiac sympathetic nerve activity

In the present study, icv injection of ghrelin did not change dialysate NE concentration. This result indicates that centrally administered ghrelin did not affect NE release into the SA node under the present experimental conditions. Central ghrelin has been shown to inhibit sympathetic nerve activity in conscious rabbits (Matsumura et al., 2002). The present study was performed under anesthetized conditions. The difference in effect on sympathetic nerve activity may be related to experimental conditions including anesthesia and artificial ventilation. Schwenke et al. (2008) reported that subcutaneous administration of ghrelin prevented the increase in cardiac sympathetic nerve activity in the acute phase after myocardial infarction. Soeki et al. (2008) also reported that sympathetic nerve activity was inhibited by subcutaneous administration of ghrelin in rats with myocardial infarction, but not in sham-operated rats. Ghrelin seems to have a stronger inhibitory effect on the activated sympathetic nervous system than on the non-activated system. The basal sympathetic tone under our experimental conditions may not have been sufficiently high to reveal the sympathoinhibitory effect of ghrelin.

The basal vagal tone could also affect the sympathoinhibitory effect of ghrelin. Lin et al. (2004) reported that microinjection of ghrelin into the NTS did not affect heart rate and reduced the response of mean arterial pressure after intravenous administration of atropine sulfate. Thus, the vagal nerve may play an important role in ghrelin-induced sympathetic suppression. The sympathoinhibitory effect of ghrelin may be partly dependent on prejunctional inhibition of NE release via muscarinic receptors associated with vagal nerve activation. In Lin's study, however, depressor response of ghrelin appeared even after atropine treatment. Thus, it is highly possible that centrally administered ghrelin has a certain sympathoinhibitory effect. We need further investigations about the sympathoinhibitory effect of ghrelin.

4.3. Methodological considerations

First, ACh is degraded by ACh esterase immediately after its release. To monitor ACh release in vivo, addition of an ACh esterase inhibitor (eserine) into the perfusate is required. In our previous study, dialysate ACh concentration correlated well with heart rate and the frequency of cervical vagal nerve stimulation in the presence of eserine (Shimizu et al., 2009). Therefore, the increase in dialysate ACh concentration by icv injection of ghrelin should reflect the activation of cardiac vagal nerve even in the presence of eserine.

Second, the eserine can also affect NE release from sympathetic nerve endings as follows. The eserine should spread around the semipermeable membrane, thereby affecting the NE release in the vicinity of the semipermeable membrane through the enhancement of muscarinic receptor mediated prejunctional inhibition.

Third, to detect changes in dialysate NE and ACh concentration sampled from the right atrium, cardiac microdialysis technique requires 20-min sampling duration. The temporal resolution may be still insufficient compared to acute changes in hemodynamics such as that observed after vagotomy in Protocol 2. The improvement of sensitivity of liquid chromatography will lead to higher temporal resolution of this technique.

Fourth, in the present study, animals were in the supine position during dialysate sampling because this experiment was performed at open-chest condition for cardiac microdialysis. The supine position may have delayed the diffusion of ghrelin and prolonged the time-lag between the injection and vagal nerve activation. Thus, the position of animals may affect the time course of hemodynamics.

4.4. Conclusion

Using cardiac microdialysis technique, we demonstrated that centrally administered ghrelin was able to activate cardiac vagal nerve. Central ghrelin may play an important role in vagal cardiovascular control.

Acknowledgments

This study was supported by the research project promoted by Ministry of Health, Labour and Welfare in Japan (H20-katsudo-Shitei-007, H21-nano-ippan-005), the Grants-in-Aid for Scientific Research promoted by Ministry of Education, Culture, Sports, Science and Technology in Japan (#20390462 and #20590242) and the Industrial Technology Research Grant Program from New Energy and Industrial Technology Development Organization (NEDO) of Japan.

References

Akiyama, T., Yamazaki, T., Ninomiya, I., 1991. In vivo monitoring of myocardial interstitial norepinephrine by dialysis technique. Am. J. Physiol. 261, H1643–H1647.
Akiyama, T., Yamazaki, T., Ninomiya, I., 1994. In vivo detection of endogenous acetylcholine release in cat ventricles. Am. J. Physiol. 266, H854–H860.
Bisi, G., Podio, V., Valetto, M.R., Broglio, F., Bertuccio, G., Del Rio, G., Arvat, E., Boghen, M.F., Deghenghi, R., Muccioli, G., Ong, H., Ghigo, E., 1999. Acute cardiovascular and hormonal effects of GH and hexarelin, a synthetic GH-releasing peptide, in humans. J. Endocrinol. Invest. 22, 266–272.
Date, Y., Murakami, N., Kojima, M., Kuroiwa, T., Matsukura, S., Kangawa, K., Nakazato, M., 2000. Central effects of a novel acylated peptide, ghrelin, on growth hormone release in rats. Biochem. Biophys. Res. Commun. 275, 477–480.
Date, Y., Nakazato, M., Murakami, N., Kojima, M., Kangawa, K., Matsukura, S., 2001. Ghrelin acts in the central nervous system to stimulate gastric acid secretion. Biochem. Biophys. Res. Commun. 280, 904–907.
Guan, X.M., Yu, H., Palyha, O.C., McKee, K.K., Feighner, S.D., Sirinathsinghji, D.J., Smith, R.G., Van der Ploeg, L.H., Howard, A.D., 1997. Distribution of mRNA encoding the growth hormone secretagogue receptor in brain and peripheral tissues. Brain Res. Mol. Brain Res. 48, 23–29.
Kamegai, J., Tamura, H., Shimizu, T., Ishii, S., Sugihara, H., Wakabayashi, I., 2001. Chronic central infusion of ghrelin increases hypothalamic neuropeptide Y and Agouti-related protein mRNA levels and body weight in rats. Diabetes 50, 2438–2443.
Kobashi, M., Shimatani, Y., Shirota, K., Xuan, S.Y., Mitoh, Y., Matsuo, R., 2006. Central neuropeptide Y induces proximal stomach relaxation via Y1 receptors in the dorsal vagal complex of the rat. Am. J. Physiol. Regul. Integr. Comp. Physiol. 290, R290–R297.
Kobashi, M., Yanagihara, M., Fujita, M., Mitoh, Y., Matsuo, R., 2009. Fourth ventricular administration of ghrelin induces relaxation of the proximal stomach in the rat. Am. J. Physiol. Regul. Integr. Comp. Physiol. 296, R217–R223.
Kojima, M., Hosoda, H., Date, Y., Nakazato, M., Matsuo, H., Kangawa, K., 1999. Ghrelin is a growth-hormone-releasing acylated peptide from stomach. Nature 402, 656–660.
Li, M., Zheng, C., Sato, T., Kawada, T., Sugimachi, M., Sunagawa, K., 2004. Vagal nerve stimulation markedly improves long-term survival after chronic heart failure in rats. Circulation 109, 120–124.
Li, Y., Wu, X., Zhao, Y., Chen, S., Owyang, C., 2006. Ghrelin acts on the dorsal vagal complex to stimulate pancreatic protein secretion. Am. J. Physiol. Gastrointest. Liver Physiol. 290, G1350–G1358.
Lin, Y., Matsumura, K., Fukuhara, M., Kagiyama, S., Fujii, K., Iida, M., 2004. Ghrelin acts at the nucleus of the solitary tract to decrease arterial pressure in rats. Hypertension 43, 977–982.
Matsumura, K., Tsuchihashi, T., Fujii, K., Abe, I., Iida, M., 2002. Central ghrelin modulates sympathetic activity in conscious rabbits. Hypertension 40, 694–699.
Nakazato, M., Murakami, N., Date, Y., Kojima, M., Matsuo, H., Kangawa, K., Matsukura, S., 2001. A role for ghrelin in the central regulation of feeding. Nature 409, 194–198.
Resmini, E., Casu, M., Patrone, V., Murialdo, G., Bianchi, F., Giusti, M., Ferone, D., Minuto, F., 2006. Sympathovagal imbalance in acromegalic patients. J. Clin. Endocrinol. Metab. 91, 115–120.

Sato, N., Kanai, S., Takano, S., Kurosawa, M., Funakoshi, A., Miyasaka, K., 2003. Central administration of ghrelin stimulates pancreatic exocrine secretion via the vagus in conscious rats. Jpn. J. Physiol. 53, 443–449.
Schwartz, P.J., De Ferrari, G.M., Sanzo, A., Landolina, M., Rordorf, R., Raineri, C., Campana, C., Revera, M., Ajmone-Marsan, N., Tavazzi, L., Odero, A., 2008. Long term vagal stimulation in patients with advanced heart failure: first experience in man. Eur. J. Heart Fail. 10, 884–891.
Schwenke, D.O., Tokudome, T., Kishimoto, I., Horio, T., Shirai, M., Cragg, P.A., Kangawa, K., 2008. Early ghrelin treatment after myocardial infarction prevents an increase in cardiac sympathetic tone and reduces mortality. Endocrinology 149, 5172–5176.
Shimizu, S., Akiyama, T., Kawada, T., Shishido, T., Yamazaki, T., Kamiya, A., Mizuno, M., Sano, S., Sugimachi, M., 2009. In vivo direct monitoring of vagal acetylcholine release to the sinoatrial node. Auton. Neurosci. 148, 44–49.
Shimizu, S., Akiyama, T., Kawada, T., Shishido, T., Mizuno, M., Kamiya, A., Yamazaki, T., Sano, S., Sugimachi, M., 2010. In vivo direct monitoring of interstitial norepinephrine levels at the sinoatrial node. Auton. Neurosci. 152, 115–118.
Soeki, T., Kishimoto, I., Schwenke, D.O., Tokudome, T., Horio, T., Yoshida, M., Hosoda, H., Kangawa, K., 2008. Ghrelin suppresses cardiac sympathetic activity and prevents early left ventricular remodeling in rats with myocardial infarction. Am. J. Physiol. Heart Circ. Physiol. 294, H426–H432.
Zigman, J.M., Jones, J.E., Lee, C.E., Saper, C.B., Elmquist, J.K., 2006. Expression of ghrelin receptor mRNA in the rat and the mouse brain. J. Comp. Neurol. 494, 528–548.

Hindawi Publishing Corporation
Journal of Drug Delivery
Volume 2011, Article ID 453619, 8 pages
doi:10.1155/2011/453619

Research Article

Cellular Injury of Cardiomyocytes during Hepatocyte Growth Factor Gene Transfection with Ultrasound-Triggered Bubble Liposome Destruction

Kazuo Komamura,[1] Rie Tatsumi,[1] Yuko Tsujita-Kuroda,[1] Takatoshi Onoe,[2] Kunio Matsumoto,[3] Toshikazu Nakamura,[3] Jun-ichi Miyazaki,[4] Takeshi Horio,[5] and Masaru Sugimachi[1]

[1] *Department of Cardiovascular Dynamics, Research Institute, National Cerebral and Cardiovascular Center, 5-7-1 Fujishiro-dai, Suita, Osaka 565-8565, Japan*
[2] *Department of Nursing Science, Taisei Gakuin University, Sakai 587-8555, Japan*
[3] *Division of Molecular Regenerative Medicine, Department of Biochemistry and Molecular Biology, Osaka University Graduate School of Medicine, Suita 565-0871, Japan*
[4] *Division of Stem Cell Regulation Research, G6, Osaka University School of Medicine, Suita 565-0871, Japan*
[5] *Division of Hypertension, National Cerebral and Cardiovascular Center, Suita 565-8565, Japan*

Correspondence should be addressed to Kazuo Komamura, kkoma@hsp.ncvc.go.jp

Received 6 August 2010; Accepted 31 October 2010

Academic Editor: Hasan Uludağ

We transfected naked HGF plasmid DNA into cultured cardiomyocytes using a sonoporation method consisting of ultrasound-triggered bubble liposome destruction. We examined the effects on transfection efficiency of three concentrations of bubble liposome (1×10^6, 1×10^7, 1×10^8/mL), three concentrations of HGF DNA (60, 120, 180 μg/mL), two insonification times (30, 60 sec), and three incubation times (15, 60, 120 min). We found that low concentrations of bubble liposome and low concentrations of DNA provided the largest amount of the HGF protein expression by the sonoporated cardiomyocytes. Variation of insonification and incubation times did not affect the amount of product. Following insonification, cardiomyocytes showed cellular injury, as determined by a dye exclusion test. The extent of injury was most severe with the highest concentration of bubble liposome. In conclusion, there are some trade-offs between gene transfection efficiency and cellular injury using ultrasound-triggered bubble liposome destruction as a method for gene transfection.

1. Introduction

Ultrasound-triggered bubble liposome destruction (sonoporation) has been proposed as a safe nonviral means of gene therapy that can target many different cells or tissues. In the field of cardiovascular medicine, this method may have significant potential for the introduction of therapeutic genes directly into vascular cells or cardiomyocytes [1, 2]. Sonoporation can only be clinically effective if the dose-effect relationship between the amount of bubble liposome and transfection efficiency is first established. However, few reports have already examined this dose-effect relationship and the safety of the procedure [3].

Transfection efficiency in sonoporation depends on various conditions including type of microbubble, mode of ultrasound, frequency of ultrasound, intensity of acoustic pressure, concentration of microbubble, dose of DNA, duration of insonification, incubation time of cell with DNA, repeat count of insonification, type of targeted cell, and other physicochemical conditions like temperature and carbon dioxide concentration, [3]. Greenleaf et al. reported that ultrasound acoustic pressure, DNA concentration, and

repeat count of insonification correlated with transfection rate [4]. Teupe et al. demonstrated that duration of insonification did not affect transfection rate [5]. Then, Chen et al. showed that transfection rate reached plateau when DNA concentration was increased [6].

Greenleaf et al. also showed that transfection rate peaked and fell off according to the change in liposome concentration [4]. They thought it might be derived from cellular toxicity of large amount of liposome. Li et al. reported that cell viability decreased along with the increase in microbubble concentration [1]. Guo et al. demonstrated that cell viability decreased with the increase in duration of insonification [7]. Suzuki et al. and Li et al. showed that cell viability decreased with the increase in ultrasound acoustic pressure [8, 9].

On the basis of those previous findings, we planned to examine the effects of amount of plasmid DNA, liposome concentration, duration of insonification, repeat count of insonification, and time of incubation with liposome, cell, and DNA on transfection rate, which was measured by means of HGF protein release into culture medium.

2. Materials and Methods

2.1. Cell Culture. Primary cultures of neonatal ventricular myocytes were prepared as described previously [10]. Briefly, apical halves of cardiac ventricles from 1-day-old Wistar rats were separated, minced, and dispersed with 0.1% collagenase type II (Worthington Biochemical Corp., Freehold, NJ). Myocytes were segregated from nonmyocytes using a discontinuous Percoll gradient (Sigma Chemical Co., Inc., St. Louis, MO). After centrifugation, the upper layer consisted of a mixed population of nonmyocyte cell types and the lower layer consisted almost exclusively of cardiac myocytes. After the myocytes had been incubated twice on uncoated 10-cm culture dishes for 30 minutes to remove any remaining nonmyocytes, the nonattached viable cells were plated on gelatin-coated 24-well culture plates or 10-cm culture dishes and then cultured in DMEM (Life Technologies, Grand Island, NY) supplemented with 10% FCS (Life Technologies, Grand Island, NY). After 24-hour incubation in DMEM with FCS, the culture medium was changed to serum-free DMEM, and all experiments were performed 24 hours later. This purification procedure has well been established [11, 12], and >95% of the cells obtained by this method were cardiomyocytes.

2.2. Plasmid DNA. Preparation of rat hepatocyte growth factor (HGF) expression plasmid DNA was described previously [13]. Briefly, rat HGF cDNA cloned by polymerase chain reaction was inserted into the unique Xho I site between the cytomegalovirus immediate-early enhancer-chicken β-actin hybrid promoter and rabbit β-globin poly A site of the pCAGGS expression plasmid [14]. The resulting plasmid, pCAGGS-HGF, was grown in Escherichia coli DH5α (Figure 1(a)). The plasmid was purified with a QUIAGEN plasmid DNA kit and dissolved in TE buffer. The purified plasmid DNA was stored at $-20°$C and diluted to the required concentration with distilled water immediately before use.

2.3. Bubble Liposome. Liposome microbubble, SHU 508A, consists of palmitic acid and galactose and provides echogenic micron-sized air bubbles when suspended in water. The diameter of bubbles ranges from 2 to 8 μm, and 97% are smaller than 6 μm [15]. These air bubbles are stabilized by palmitic acid, which forms a molecular film that lowers the surface tension of the aqueous vehicle. The SHU 508A bubbles are nontoxic, have a neutral pH, are biodegradable, and are made from a physiologically occurring substance. The physiochemical properties of SHU 508A bubbles are typical of a saccharide solution [15].

2.4. Experiment on Ultrasound Mode. Before performing the experiments for dose-effect relationships using liposome sonoporation, we needed to determine the most appropriate ultrasound mode for the sonoporation procedure for efficient transfection. We tested four modes of ultrasound: pulsed wave Doppler, color flow Doppler, continuous wave Doppler, and harmonic power Doppler, which are available with standard echocardiographic machinery in a clinical laboratory. We performed a simple transfection experiment at the same acoustic pressure of 0.5 W/cm^2 for each ultrasound mode, using a single condition with 60 μg HGF plasmid DNA, 1×10^7 particles/mL of SHU 508A liposome, 30 sec insonification, 15 min of DNA incubation, and 3 repetitions of insonification.

Rat neonatal cardiomyocytes were inoculated and grown to confluence in DMEM+10% FCS. After confluence had been reached in a 35 mm Petri dish, the medium was changed to fresh defined serum-free medium. Plasmid DNA was diluted with distilled water immediately before the transfection. Each experiment was performed on 20 dishes. Cells on each dish were treated with ultrasound (Figure 1(b)). Pulsed wave Doppler, color flow Doppler, and continuous wave Doppler were insonified from PSK-25AT acoustic transducer with Toshiba SSA-380A (Toshiba Medical Systems), and harmonic power Doppler was insonified from S3 transducer with Sonos 5500 (Phillips Medical Systems). The experimental results are shown in Figure 2. Continuous-wave Doppler ultrasound was the most efficacious and was used for subsequent experiments.

2.5. Experiments for Dose-Effect Relations. The medium in 35 mm Petri dishes containing the cardiomyocytes was changed to fresh defined serum-free medium from DMEM+10% FCS. Rat HGF plasmid DNA was diluted with distilled water, and a volume corresponding to 60, 120, or 180 μg was added to each of the 20 Petri dishes per DNA dose. Cells on each dish were then treated with continuous-wave Doppler ultrasound (frequency of 2.5 MHz and acoustic intensity of 0.5 W/cm^2 from a PSK-25AT acoustic transducer with Toshiba SSA-380A Ultrasound system) with SHU 508A liposome (1×10^7 particles/mL) for acoustic exposure time of 30 or 60 seconds at room temperature (Figure 1(b)). In a separate series of experiments, we tested four liposome

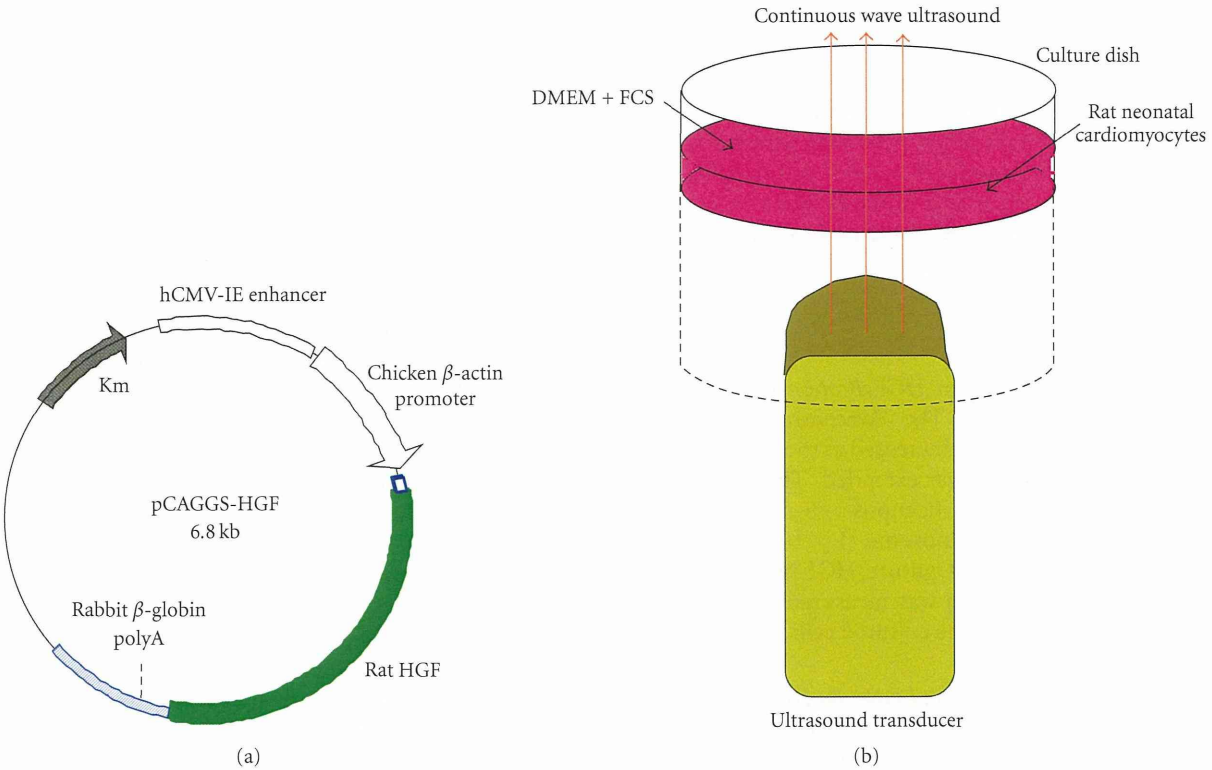

FIGURE 1: (a) Structure of the expression plasmid pCAGGS-HGF. The expression cassette of pCAGGS-HGF contains chicken β-actin promoter, rat HGF, and rabbit β-globin poly A. (b) Experimental setup. The transducer was attached to the bottom of the dish.

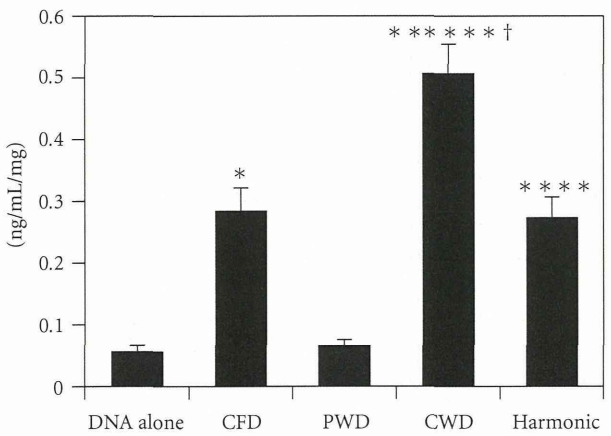

FIGURE 2: Comparison of four modes of ultrasound for sonoporation. Cells treated with continuous-wave Doppler ultrasound yielded the largest amount of HGF protein indicating this to be the most effective ultrasound mode. CFD: color flow Doppler; PWD: pulsed wave Doppler; CWD: continuous wave Doppler; Harmonic: harmonic power Doppler. $^{*}P < .05$ versus DNA alone; $^{**}P < .05$ versus CFD; $^{***}P < .05$ versus PWD; $^{\dagger}P < .05$ versus Harmonic.

concentrations (0, 1×10^6, 1×10^7 or 1×10^8 particles/mL), three insonification repetitions (1 insonification only, 3 or 5 insonifications for 30 seconds), and three DNA incubation times (15, 60 or 120 min). After the incubation, the culture medium was changed to normal DMEM+10% FCS and the cells were cultured for 72 hours. In a separate set of experiments, we examined the effect of culture period on the amount of DNA product that is HGF protein by discontinuing culture at 24, 48, and 72 hours and measuring the amount of rat HGF protein in the medium. The total amount of protein content in the cultured cells was measured and used to correct the HGF level in each dish. We measured rat HGF protein using an EIA kit (Institute of Immunology Co., Ltd., Tokyo, Japan) [13] and protein content of cultured cells using a Modified Lowry Protein Assay Kit (Pierce Biotechnology, Rockford).

2.6. Viability of Cultured Cells. To determine the safety of sonoporation, in a separate experiment, cultured cells were exposed to 0.1% trypan blue for 5 min just after ultrasound insonification. This allowed assessment of sarcolemmal membrane damage and was performed for each concentration of liposome, each insonification time, and each number of repetitions of insonification. The number of stained and unstained cells in the dishes was counted and used to calculate the percentage of intact cells [16]. The degree of cellular injury caused by sonoporation was determined by examining the insonified cells by scanning electron microscopy (Hitachi S-4800). Immediately after ultrasound insonification in the presence of liposome, the cardiomyocytes were fixed with phosphate-buffered 2.5% glutaraldehyde for 4 hours, followed by postfixation with 1%

osmium tetroxide for 1 hour, and then were conventionally prepared for scanning electron microscopy.

2.7. Statistical Analysis. Data were expressed as the mean ± SEM. Comparisons of parameters from experimental groups were performed with unpaired t tests and resulting P-values were corrected according to the Bonferroni method. In analyses, $P < .05$ was considered to indicate statistical significance.

3. Results

3.1. Effect of Culture Period on HGF Protein Production by Sonoporated Cardiomyocytes. The concentration of HGF protein in the culture medium increased as the culture period after ultrasonic transfection was extended. The transfection consisted of three 30-sec insonifications a 15-min incubation with HGF DNA (60 μg) and liposome (1×10^7 particle/mL) (Figure 3(a)). After 72 hours of culture, HGF protein concentration in the culture medium was measured and corrected using the protein content of the cultured cells.

3.2. Effect of the Amount of Plasmid DNA on HGF Protein Production by Sonoporated Cardiomyocytes. HGF protein concentration in the culture medium was 0.54 ± 0.049 ng/mL/mg and was highest when 60 μg of DNA was administered with a liposome concentration of 1×10^7 particles/mL, a15-min incubation, and three 30-sec insonification. Although the nominal mean values of HGF protein after transfection of 120 and 180 μg DNA were lower than those after transfection of 60 μg, the differences were not statistically significant (Figure 3(b)).

3.3. Effect of Incubation Period with Plasmid DNA and Liposome on HGF Protein Production by Sonoporated Cardiomyocytes. HGF protein concentration in the culture medium was 0.56 ± 0.053 ng/mL/mg and was highest when the incubation time was 15 min with a liposome concentration of 1×10^7 particles/mL, 60 μg DNA, and three 30-sec insonification. Although the mean values of HGF protein after transfection for 60 and 120 min were lower than those after 15 min incubation, the differences were not statistically significant (Figure 3(c)).

3.4. Effect of Insonification Time on HGF Protein Production by Sonoporated Cardiomyocytes. HGF protein concentration in the culture medium was 0.59 ± 0.052 ng/mL/mg and was highest when the insonification period was 30 sec with 60 μg DNA, a liposome concentration of 1×10^7 particles/mL, and 15-min incubation. There was no significant difference in HGF production in cells insonified for 30 and 60 min (Figure 3(d)).

3.5. Effect of Liposome Concentration on HGF Protein Production by Sonoporated Cardiomyocytes. HGF protein concentration in the culture medium was 0.53 ± 0.053 ng/mL/mg and was nominally highest when the liposome concentration was 1×10^7 particles/mL and insonification consisted of three 30-sec ultrasound exposures, though it was statistically similar to that obtained with 1×10^6 particles/mL. At a higher liposome concentration of 1×10^8 particles/mL, HGF protein concentration decreased (Figure 3(e)).

3.6. Effect of Repetition of Insonification on HGF Protein Production by Sonoporated Cardiomyocytes. HGF protein concentration in the culture medium was 0.54 ± 0.053 ng/mL/mg and was highest when three 30-sec insonifications were given, with a liposome concentration of 1×10^7 particles/mL and 60 mg DNA. This protein production was statistically higher than in cells given one or five insonifications (Figure 3(f)).

3.7. Effect of Insonification Time on Cell Viability. The percentage of dead cells was 14.7 ± 0.9% and was higher in the cells given five 30-sec insonifications at a liposome concentration of 1×10^7 particles/mL (Figure 4(a)). There was no statistical difference between 30- and 60-sec insonification.

3.8. Effect of Liposome Concentration on Cell Viability. The percentage of dead cells increased with increasing concentrations of liposome (Figure 4(b)). The dead cell count was 24.8 ± 2.9% and was highest when the liposome concentration was 1×10^8 particles/mL and three 30-sec insonifications were used.

3.9. Effect of Number of Insonification Repetitions on Cell Viability. The percentage of dead cells increased as the number of insonification repetitions increased (Figure 4(c)). The dead cell count was 14.7 ± 0.9% and was highest when five repetitions of the insonification step were given, with a liposome concentration of 1×10^7 particles/mL.

3.10. Scanning Electron Microscopy Observations of Sonoporated Cardiomyocytes. No particular changes were evident on the surfaces of untreated control cultured cardiomyocytes when viewed with the scanning electron microscope at low and high magnification (Figures 5(a) and 5(b)). After sonoporation with a low concentration of liposome (Figure 5(c)) and with a high concentration of liposome (Figure 5(d)), microdimples or pores were observed on the surfaces of the cultured cardiomyocytes.

4. Discussion

Considerable efforts have been made to develop methods that will allow effective and safe introduction of vectors into cells for gene therapy. However, we still need a breakthrough in the form of a novel vector that will transform cells at high efficiency and with low risk of adverse effects. This is especially true in cardiovascular medicine, where malignant cellular transformation is rare [17]. One of the promising candidates for safe and efficacious gene transfection is a naked plasmid vector that has been modified to have high affinity for cardiovascular tissues but which has no built-in viral components [17, 18]. We have developed a method for electroporation of a cytokine gene for treatment of

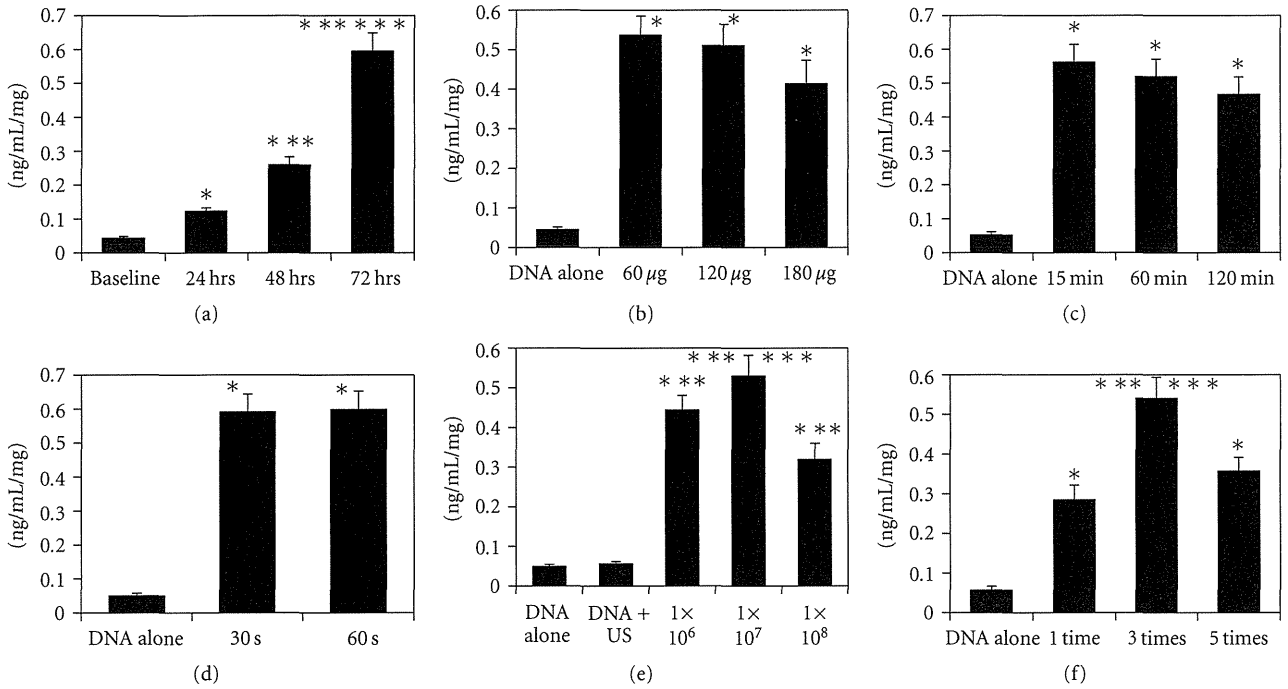

FIGURE 3: (a) Effect of culture period after transfection of HGF DNA on HGF protein production using 60 μg of DNA and 1×10^7 particles/mL liposome with three 30-sec insonifications and 15-min incubation with DNA. Baseline was the concentration of rat HGF protein in the culture medium around rat cardiomyocytes without any intervention at the beginning of cell culture. $^*P < .05$ versus baseline; $^{**}P < .05$ versus 24 hours after the onset of culture; $^{***}P < .05$ versus 48 hours after the onset of culture. (b) Effect of amount of plasmid DNA on HGF protein production using 1×10^7 particles/mL liposome with three 30-sec insonifications and 15-min incubation with DNA. "DNA alone" indicates the concentration of rat HGF protein in the culture medium of cardiomyocytes treated with 60 μg DNA without insonification. $^*P < .05$ versus DNA alone. (c) Effect of incubation period of cardiomyocytes with plasmid DNA and liposome on HGF protein production using 60 μg of DNA and 1×10^7 particles/mL liposome with three 30-sec insonifications. $^*P < .05$ versus DNA alone. (d) Effect of insonification time on protein production using 60 μg of DNA, 1×10^7 particles/mL liposome, and 15-min incubation with DNA, and three 30- or 60-sec insonifications. $^*P < .05$ versus DNA alone. (e) Effect of liposome concentration on HGF protein production using 60 μg of DNA with three 30-sec insonifications and 15-min incubation with DNA. $^*P < .05$ versus DNA alone; $^{**}P < .05$ versus 0 particles/mL; $^{***}P < .05$ versus 1×10^8 particles/mL. (f) Effect of repetition of insonification on HGF protein production using 6 μg of DNA and 1×10^7 particles/mL liposome with 15-min incubation with DNA. $^*P < .05$ versus DNA alone; $^{**}P < .05$ versus 1 time; $^{***}P < .05$ versus 5 times.

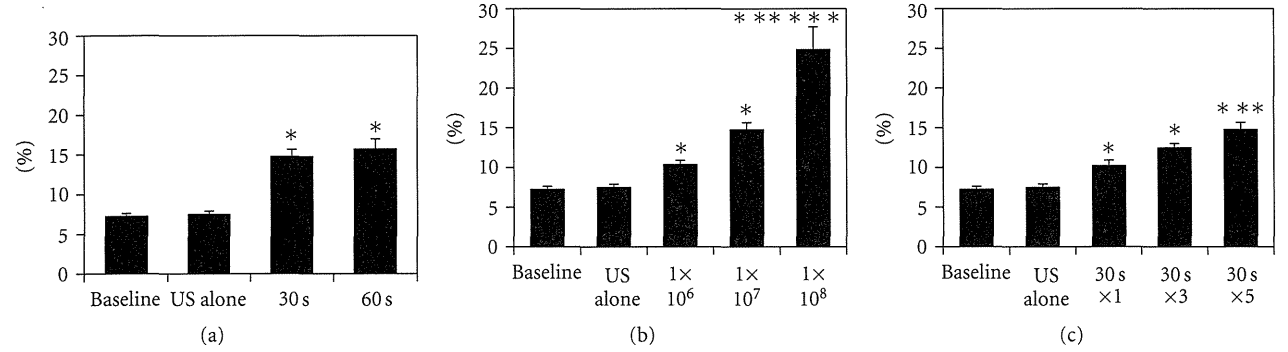

FIGURE 4: (a) Effect of insonification time on cell viability using 60 μg of DNA, 1×10^7 particles/mL liposome, and 15-min incubation with DNA, and three 30- or 60-sec insonifications. "US alone" represents the percentage of dead cells immediately after three 30-sec insonifications in the absence of liposome and DNA. $^*P < .05$ versus baseline. (b) Effect of liposome concentration on cell viability using 60 μg of DNA and three 30-sec insonifications and 15-min incubation with DNA. $^*P < .05$ versus baseline; $^{**}P < .05$ versus 1×10^6 particles/mL; $^{***}P < .05$ versus 1×10^8 particles/mL. (c) Effect of repetitions of insonification on cell viability using 60 μg of DNA, 1×10^7 particles/mL liposome, and 15-min incubation with DNA. $^*P < .05$ versus baseline; $^{**}P < .05$ versus 30 sec $\times$ 1.

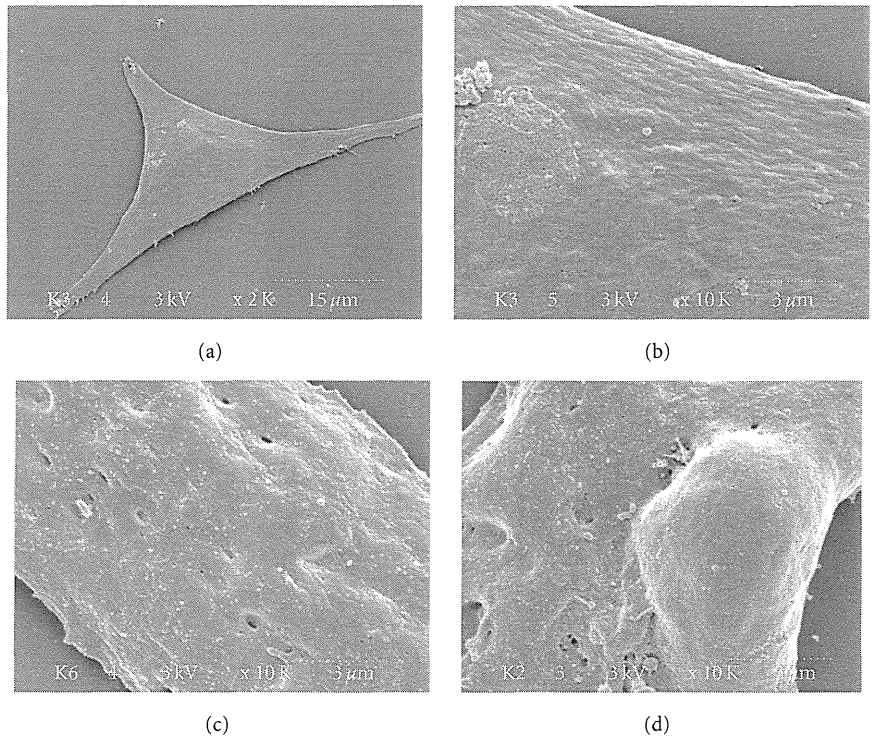

(a) (b) (c) (d)

FIGURE 5: (a) and (b) Scanning electron microscopic images of intact cell surfaces of cultured cardiomyocytes. Scale dots are indicated on the images. (c) Image of a cell surface immediately after sonoporation using 1×10^6 particles/mL liposome. (d) Image of a cell surface immediately after sonoporation using 1×10^8 particles/mL liposome.

cardiomyopathy [13]. However, using electric shock for transfection is not clinically practical. For this reason, we are pursuing the present sonoporation method as a protocol for gene transfection.

The HGF protein used in the present study is found in a wide variety of cell types and has multiple biological properties, including mitogenic, motogenic, morphogenic and antiapoptotic activities [19]. Several lines of evidence indicate that this molecule has potential for therapeutic use for treatment of heart failure, myocardial infarction, angina, and hypertension [20–22]. HGF may also have enormous therapeutic potential for hepatic and renal disorders, in addition to cardiovascular diseases [23–26].

In the present study, we showed variations in amount of HGF plasmid DNA, liposome concentration, the duration of insonification, and incubation time of the cardiomyocytes with liposome and DNA, and their dose relationships with the final amount of HGF protein released from the cultured neonatal cardiomyocytes. We found that specific amounts of liposome and repetitions of insonification were needed for effective protein production from cardiomyocytes. However, high concentrations of bubble liposome and large numbers of repeat insonifications resulted in decreased cell viability.

Plasma membrane sonoporation induced by ultrasound and subsequent self-sealing has been reported in previous investigations [27–29]. However, the exact mechanism by which membrane sonoporation causes substance incorporation into the cell is not yet understood. Some investigators speculate that the membrane poration results in both transfection efficiency and cellular damage. In the present study, scanning microscopy images revealed some microdimples or pores on the cell surface after sonoporation, which did not exist on the surface of control cardiomyocytes. The numbers of dimples or pores tended to increase with higher concentrations of liposome. Thus, we speculate that these dimples or pores on the cell surface might be related to transfection efficiency and might be evidence of cellular injury by sonoporation. Previous studies of sonoporation of vascular walls revealed that microbubble destruction would cause rupture of microvessels and extravasation [30–33], which would cancel out some benefits of sonoporation. Thus, the poration and self-sealing mechanism needs to be fully investigated and optimized.

A sonoporation technique targeting the cardiovascular system has now been developed for gene transfection to myocardium, limb skeletal muscle, and arteries [34–37]. For a variety of target tissues, a number of microbubbles, including liposomes, and a range of ultrasound modes have been developed. The optimal combination of the type of microbubble, ultrasound mode, and target tissue still needs to be resolved [38–40]. However, the principal types of ultrasound used for sonoporation have included pulsed wave Doppler or continuous wave Doppler with acoustic pressure ranging 0.5–5 W/cm^2 [34–37]. In the present study, we found that continuous wave Doppler at a standard frequency for clinical use, that is, 2.5 MHz and the usual acoustic pressure of 0.5 W/cm^2, was most effective with our cardiomyocytes.

The reason we used one of the standard ultrasound modes with standard settings for clinical use is that we would like to use our sonoporation system eventually in a clinical setting.

The present study has several limitations. To avoid the complexity of numerous combinations of experimental conditions, such as amount of DNA, concentration of liposome, duration of insonification, repeat count of insonification, length of incubation time, and culture period after gene transfection, we only used several practical combinations for an in vitro experiment for cultured cardiomyocytes. Thus, we might have missed other multimodal aspects of dose-effect relationships among these conditions.

5. Conclusion

HGF DNA was successfully transferred to cultured cardiomyocytes using sonoporation with a defined liposome concentration and a mode of insonification. A number of trade-offs between transfection efficiency and cellular injury have to be balanced to optimize this sonoporation method.

Acknowledgments

This study was supported by a Grant-in-Aid for Scientific Research 14570709 from the Ministry of Education, Culture, Sport, Science, and Technology of Japan and by the Program for Promotion of Fundamental Studies in Health Sciences of the Pharmaceuticals and Medical Devices Agency (PMDA).

References

[1] T. Li, K. Tachibana, M. Kuroki, and M. Kuroki, "Gene transfer with echo-enhanced contrast agents: comparison between Albunex, Optison, and Levovist in mice—initial results," *Radiology*, vol. 229, no. 2, pp. 423–428, 2003.

[2] S. Tsunoda, O. Mazda, Y. Oda et al., "Sonoporation using microbubble BR14 promotes pDNA/siRNA transduction to murine heart," *Biochemical and Biophysical Research Communications*, vol. 336, no. 1, pp. 118–127, 2005.

[3] L. B. Feril Jr. and T. Kondo, "Biological effects of low intensity ultrasound: the mechanism involved, and its implications on therapy and on biosafety of ultrasound," *Journal of Radiation Research*, vol. 45, no. 4, pp. 479–489, 2004.

[4] W. J. Greenleaf, M. E. Bolander, G. Sarkar, M. B. Goldring, and J. F. Greenleaf, "Artificial cavitation nuclei significantly enhance acoustically induced cell transfection," *Ultrasound in Medicine and Biology*, vol. 24, no. 4, pp. 587–595, 1998.

[5] C. Teupe, S. Richter, B. Fisslthaler et al., "Vascular gene transfer of phosphomimetic endothelial nitric oxide synthase (S1177D) using ultrasound-enhanced destruction of plasmid-loaded microbubbles improves vasoreactivity," *Circulation*, vol. 105, no. 9, pp. 1104–1109, 2002.

[6] S. Chen, R. V. Shohet, R. Bekeredjian, P. Frenkel, and P. A. Grayburn, "Optimization of ultrasound parameters for cardiac gene delivery of adenoviral or plasmid deoxyribonucleic acid by ultrasound-targeted microbubble destruction," *Journal of the American College of Cardiology*, vol. 42, no. 2, pp. 301–308, 2003.

[7] D.-P. Guo, X.-Y. Li, P. Sun et al., "Ultrasound-targeted microbubble destruction improves the low density lipoprotein receptor gene expression in HepG2 cells," *Biochemical and Biophysical Research Communications*, vol. 343, no. 2, pp. 470–474, 2006.

[8] R. Suzuki, T. Takizawa, Y. Negishi, N. Utoguchi, and K. Maruyama, "Effective gene delivery with novel liposomal bubbles and ultrasonic destruction technology," *International Journal of Pharmaceutics*, vol. 354, no. 1-2, pp. 49–55, 2008.

[9] H. L. Li, X. Z. Zheng, H. P. Wang, F. Li, Y. Wu, and L. F. Du, "Ultrasound-targeted microbubble destruction enhances AAV-mediated gene transfection in human RPE cells in vitro and rat retina in vivo," *Gene Therapy*, vol. 16, no. 9, pp. 1146–1153, 2009.

[10] T. Horio, T. Nishikimi, F. Yoshihara, H. Matsuo, S. Takishita, and K. Kangawa, "Inhibitory regulation of hypertrophy by endogenous atrial natriuretic peptide in cultured cardiac myocytes," *Hypertension*, vol. 35, no. 1, part 1, pp. 19–24, 2000.

[11] J.-S. Zheng, M. O. Boluyt, L. O'Neill, M. T. Crow, and E. G. Lakatta, "Extracellular ATP induces immediate-early gene expression but not cellular hypertrophy in neonatal cardiac myocytes," *Circulation Research*, vol. 74, no. 6, pp. 1034–1041, 1994.

[12] M. Harada, H. Itoh, O. Nakagawa et al., "Significance of ventricular myocytes and nonmyocytes interaction during cardiocyte hypertrophy: evidence for endothelin-1 as a paracrine hypertrophic factor from cardiac nonmyocytes," *Circulation*, vol. 96, no. 10, pp. 3737–3744, 1997.

[13] K. Komamura, R. Tatsumi, J.-I. Miyazaki et al., "Treatment of dilated cardiomyopathy with electroporation of hepatocyte growth factor gene into skeletal muscle," *Hypertension*, vol. 44, no. 3, pp. 365–371, 2004.

[14] K. Matsumoto and T. Nakamura, "Hepatocyte growth factor (HGF) as a tissue organizer for organogenesis and regeneration," *Biochemical and Biophysical Research Communications*, vol. 239, no. 3, pp. 639–644, 1997.

[15] B. B. Goldberg, JI. B. Liu, and F. Forsberg, "Ultrasound contrast agents: a review," *Ultrasound in Medicine and Biology*, vol. 20, no. 4, pp. 319–333, 1994.

[16] S. Kato, G. Takemura, R. Maruyama et al., "Apoptosis, rather than oncosis, is the predominant mode of spontaneous death of isolated adult rat cardiac myocytes in culture," *Japanese Circulation Journal*, vol. 65, no. 8, pp. 743–748, 2001.

[17] O. J. Müller, H. A. Katus, and R. Bekeredjian, "Targeting the heart with gene therapy-optimized gene delivery methods," *Cardiovascular Research*, vol. 73, no. 3, pp. 453–462, 2007.

[18] C. A. Holladay, T. O'Brien, and A. Pandit, "Non-viral gene therapy for myocardial engineering," *Wiley Interdisciplinary Reviews: Nanomedicine and Nanobiotechnology*, vol. 2, no. 3, pp. 232–248, 2010.

[19] K. Matsumoto and T. Nakamura, "Hepatocyte growth factor (HGF) as a tissue organizer for organogenesis and regeneration," *Biochemical and Biophysical Research Communications*, vol. 239, no. 3, pp. 639–644, 1997.

[20] K. Matsumoto and T. Nakamura, "HGF: its organotrophic role and therapeutic potential," *CIBA Foundation Symposia*, no. 212, pp. 198–211, 1997.

[21] N. Tomita, R. Morishita, J. Higaki, and T. Ogihara, "Novel molecular therapeutic approach to cardiovascular disease based on hepatocyte growth factor," *Journal of Atherosclerosis and Thrombosis*, vol. 7, no. 1, pp. 1–7, 2000.

[22] K. Komamura, J. Miyazaki, E. Imai, K. Matsumoto, T. Nakamura, and M. Hori, "Hepatocyte growth factor gene therapy for hypertension," *Methods in Molecular Biology*, vol. 423, pp. 393–404, 2008.

[23] K.-I. Kosai, K. Matsumoto, S. Nagata, Y. Tsujimoto, and T. Nakamura, "Abrogation of Fas-induced fulminant hepatic

failure in mice by hepatocyte growth factor," *Biochemical and Biophysical Research Communications*, vol. 244, no. 3, pp. 683–690, 1998.

[24] T. Ueki, Y. Kaneda, H. Tsutsui et al., "Hepatocyte growth factor gene therapy of liver cirrhosis in rats," *Nature Medicine*, vol. 5, no. 2, pp. 226–230, 1999.

[25] S. Mizuno, K. Matsumoto, and T. Nakamura, "HGF as a renotrophic and anti-fibrotic regulator in chronic renal disease," *Frontiers in Bioscience*, vol. 13, pp. 7072–7086, 2008.

[26] K. Matsumoto and T. Nakamura, "Hepatocyte growth factor: renotropic role and potential therapeutics for renal diseases," *Kidney International*, vol. 59, no. 6, pp. 2023–2038, 2001.

[27] K. Tachibana, T. Uchida, K. Ogawa, N. Yamashita, and K. Tamura, "Induction of cell-membrane porosity by ultrasound," *The Lancet*, vol. 353, no. 9162, p. 1409, 1999.

[28] S. Mehier-Humbert, T. Bettinger, F. Yan, and R. H. Guy, "Plasma membrane poration induced by ultrasound exposure: implication for drug delivery," *Journal of Controlled Release*, vol. 104, no. 1, pp. 213–222, 2005.

[29] F. Yang, N. Gu, D. Chen et al., "Experimental study on cell self-sealing during sonoporation," *Journal of Controlled Release*, vol. 131, no. 3, pp. 205–210, 2008.

[30] D. M. Skyba, R. J. Price, A. Z. Linka, T. C. Skalak, and S. Kaul, "Direct in vivo visualization of intravascular destruction of microbubbles by ultrasound and its local effects on tissue," *Circulation*, vol. 98, no. 4, pp. 290–293, 1998.

[31] J. Song, J. C. Chappell, M. Qi, E. J. VanGieson, S. Kaul, and R. J. Price, "Influence of injection site, microvascular pressure and ultrasound variables on microbubble-mediated delivery of microspheres to muscle," *Journal of the American College of Cardiology*, vol. 39, no. 4, pp. 726–731, 2002.

[32] S. Hernot and A. L. Klibanov, "Microbubbles in ultrasound-triggered drug and gene delivery," *Advanced Drug Delivery Reviews*, vol. 60, no. 10, pp. 1153–1166, 2008.

[33] M. R. Böhmer, C. H. T. Chlon, B. I. Raju, C. T. Chin, T. Shevchenko, and A. L. Klibanov, "Focused ultrasound and microbubbles for enhanced extravasation," *Journal of Controlled Release*, vol. 148, no. 1, pp. 18–24, 2010.

[34] I. Rosenthal, J. Z. Sostaric, and P. Riesz, "Sonodynamic therapya review of the synergistic effects of drugs and ultrasound," *Ultrasonics Sonochemistry*, vol. 11, no. 6, pp. 349–363, 2004.

[35] J. M. Tsutsui, F. Xie, and R. T. Porter, "The use of microbubbles to target drug delivery," *Cardiovascular Ultrasound*, vol. 2, article 23, 2004.

[36] C. M. H. Newman and T. Bettinger, "Gene therapy progress and prospects: ultrasound for gene transfer," *Gene Therapy*, vol. 14, no. 6, pp. 465–475, 2007.

[37] C. R. Mayer and R. Bekeredjian, "Ultrasonic gene and drug delivery to the cardiovascular system," *Advanced Drug Delivery Reviews*, vol. 60, no. 10, pp. 1177–1192, 2008.

[38] S. Hernot and A. L. Klibanov, "Microbubbles in ultrasound-triggered drug and gene delivery," *Advanced Drug Delivery Reviews*, vol. 60, no. 10, pp. 1153–1166, 2008.

[39] S. Tinkov, R. Bekeredjian, G. Winter, and C. Coester, "Microbubbles as ultrasound triggered drug carriers," *Journal of Pharmaceutical Sciences*, vol. 98, no. 6, pp. 1935–1961, 2009.

[40] C.-Y. Lin, T.-M. Liu, C.-Y. Chen et al., "Quantitative and qualitative investigation into the impact of focused ultrasound with microbubbles on the triggered release of nanoparticles from vasculature in mouse tumors," *Journal of Controlled Release*, vol. 146, no. 3, pp. 291–298, 2010.

J Physiol 589.7 (2011) pp 1769–1790

The Journal of Physiology

Closed-loop spontaneous baroreflex transfer function is inappropriate for system identification of neural arc but partly accurate for peripheral arc: predictability analysis

Atsunori Kamiya, Toru Kawada, Shuji Shimizu and Masaru Sugimachi

Department of Cardiovascular Dynamics, National Cerebral and Cardiovascular Center Research Institute, Suita-city, Osaka 565-8565, Japan

Non-technical summary The arterial baroreflex is a closed-loop, negative feedback control system that senses baroreceptor pressure and controls systemic arterial pressure (AP) to attenuate perturbations in AP. The total arc of the baroreflex consists of two subsystems: the neural (baroreceptor pressure input to sympathetic nerve activity (SNA)) and peripheral (SNA input to AP) arcs. We show that although the spontaneous baroreflex transfer function obtained by closed-loop analysis has been believed to represent the neural arc function, it is inappropriate for system identification of the neural arc but is essentially appropriate for the peripheral arc under resting condition, when compared with open-loop transfer functions that have good predictabilities of time-series output dynamics from input signals. Our results indicate that in the spontaneous baroreflex system under closed-loop conditions, the peripheral arc (feedforward) function predominates over the neural arc (feedback) function, probably because of the SNA component that is independent of the baroreceptor pressure input.

Abstract Although the dynamic characteristics of the baroreflex system have been described by baroreflex transfer functions obtained from open-loop analysis, the predictability of time-series output dynamics from input signals, which should confirm the accuracy of system identification, remains to be elucidated. Moreover, despite theoretical concerns over closed-loop system identification, the accuracy and the predictability of the closed-loop spontaneous baroreflex transfer function have not been evaluated compared with the open-loop transfer function. Using urethane and α-chloralose anaesthetized, vagotomized and aortic-denervated rabbits ($n = 10$), we identified open-loop baroreflex transfer functions by recording renal sympathetic nerve activity (SNA) while varying the vascularly isolated intracarotid sinus pressure (CSP) according to a binary random (white-noise) sequence (operating pressure $\pm$ 20 mmHg), and using a simplified equation to calculate closed-loop-spontaneous baroreflex transfer function while matching CSP with systemic arterial pressure (AP). Our results showed that the open-loop baroreflex transfer functions for the neural and peripheral arcs predicted the time-series SNA and AP outputs from measured CSP and SNA inputs, with r^2 of 0.8 ± 0.1 and 0.8 ± 0.1, respectively. In contrast, the closed-loop-spontaneous baroreflex transfer function for the neural arc was markedly different from the open-loop transfer function (enhanced gain increase and a phase lead), and did not predict the time-series SNA dynamics (r^2; 0.1 ± 0.1). However, the closed-loop-spontaneous baroreflex transfer function of the peripheral arc partially matched the open-loop transfer function in gain and phase functions, and had limited but reasonable predictability of the time-series AP dynamics (r^2, 0.7 ± 0.1). A numerical simulation suggested that a noise predominantly in the neural arc under resting conditions might be a possible mechanism responsible for our findings. Furthermore, the predictabilities of the neural arc transfer functions obtained in open-loop and closed-loop conditions were validated by closed-loop pharmacological (phenylephrine and nitroprusside infusions) pressure interventions. Time-series SNA responses

DOI: 10.1113/jphysiol.2011.203455

to drug-induced AP changes predicted by the open-loop transfer function matched closely the measured responses (r^2, 0.9 ± 0.1), whereas SNA responses predicted by closed-loop-spontaneous transfer function deviated greatly and were the inverse of measured responses (r, -0.8 ± 0.2). These results indicate that although the spontaneous baroreflex transfer function obtained by closed-loop analysis has been believed to represent the neural arc function, it is inappropriate for system identification of the neural arc but is essentially appropriate for the peripheral arc under resting conditions, when compared with open-loop analysis.

(Resubmitted 2 December 2010; accepted after revision 7 February 2011; first published online 14 February 2011)
Corresponding author A. Kamiya: Department of Cardiovascular Dynamics, National Cerebral and Cardiovascular Center Research Institute, 5-7-1 Fujishirodai, Suita, Osaka 565-8565, Japan. Email: kamiya@ri.ncvc.go.jp

Abbreviations AP, arterial pressure; CSP, intra-carotid sinus pressure; *r*linear correlation coefficient; RMS, root mean square; SNA, sympathetic nerve activity.

Introduction

The arterial baroreflex plays a crucial role in circulatory control by its dynamic system characteristics (Eckberg & Sleight, 1992; Rowell, 1993). The baroreflex is a closed-loop, negative feedback control system that constantly senses arterial pressure (AP) by baroreceptors and quickly regulates systemic AP physiologically to attenuate perturbations in AP (Eckberg & Sleight, 1992; Rowell, 1993). The total arc baroreflex system consists of two subsystems: the neural and peripheral arcs (Kamiya *et al.* 2005*b*, 2008*a*, 2010; Kawada *et al.* 2010). The neural arc subsystem represents central processing from baroreceptor pressure to efferent sympathetic nerve activity (SNA), whereas the peripheral arc subsystem represents processing from SNA to systemic AP via peripheral circulatory organs including heart, kidney and blood vessels (Fig. 1) (Ikeda *et al.* 1996; Kamiya *et al.* 2005*b*).

Transfer function analysis is a powerful tool to determine the dynamic characteristics of biosystems. This analysis has revealed the dynamic causality mainly in 'open-loop' biosystems, including cerebral autoregulation (Zhang *et al.* 2002), renal vascular function (DiBona & Sawin, 2003, 2004), heart rate control (Ikeda *et al.* 1995) and cutaneous circulation (Kamiya *et al.* 2008*b*). We have applied the transfer function analysis to characterize the 'closed-loop' arterial baroreflex system, in which we used the open-loop and white-noise pressure perturbation techniques to overcome the difficulties of closed-loop system identification (see Appendix A) (Ikeda *et al.* 1996; Kawada *et al.* 2002; Kamiya *et al.* 2005*b*, 2008*a*). We have reported that the neural arc transfer function (H_n) has derivative and high-cut filter characteristics with a pure delay, indicating that more rapid change of arterial pressure results in greater response of SNA to pressure change (Kawada *et al.* 2002; Kamiya *et al.* 2005*b*), whereas the peripheral arc transfer function (H_p) has second-order low-pass filter characteristics with a pure delay (see Appendix B) (Kawada *et al.* 2002; Kamiya *et al.* 2005*b*). However, at least two important issues remain to be elucidated.

First, a hallmark of the transfer function, the predictability of time-series output dynamics from input signals (Ikeda *et al.* 1995; Kamiya *et al.* 2008*b*), has not yet been investigated in the baroreflex system. Accurate system identification of the transfer function yields good predictability, whereas inappropriate system identification results in poor predictability. In the present study, we tested the first hypothesis that the open-loop baroreflex transfer functions of the neural and peripheral arcs are capable of predicting time-series SNA and AP output dynamics from baroreceptor pressure and SNA inputs, respectively.

Second, identifying transfer functions is theoretically difficult under closed-loop and spontaneous resting baroreflex conditions. The reason is that unknown noises in the neural and peripheral arcs would interfere with the accuracy of system identification in closed-loop-spontaneous conditions, in contrast to open-loop transfer function identification where the interfering effects of noises would be eliminated by the open-loop and white-noise pressure perturbation techniques (Ikeda *et al.* 1996; Kawada *et al.* 2002; Kamiya *et al.* 2005*b*, 2008*a*) (see Appendix A). Although earlier interesting studies have applied a simplified (open-loop-like) calculation of transfer function to closed-loop-spontaneous resting baroreflex condition in humans (Cooke *et al.* 1999, 2009; Ogoh *et al.* 2009) and animals (Orea *et al.* 2007) without opening the loop, whether the reported transfer functions are actually capable of predicting time-series output dynamics has not been verified. In addition, the accuracy and limitation of closed-loop-spontaneous baroreflex transfer functions remain unclear from the viewpoint of comparing with open-loop transfer functions. In the present study, we tested the second hypothesis that the closed-loop-spontaneous baroreflex transfer function is limited to predict baroreflex dynamics compared with the open-loop transfer function.

In the present study, by artificially controlling intra-carotid sinus pressure (CSP) and recording renal SNA and systemic AP, we identified the open-loop baroreflex transfer functions by introducing CSP perturbation according to a binary random (white-noise) sequence. We also determined the closed-loop-spontaneous baroreflex transfer functions by matching CSP with systemic AP. We then compared the characteristics and predictability of these transfer functions. Our results confirmed good predictability of the open-loop baroreflex transfer functions, and unexpectedly indicated that the closed-loop-spontaneous transfer function approximately matched the open-loop transfer function for the peripheral arc but deviated markedly from the open-loop transfer function for the neural arc. Thus, the closed-loop-spontaneous baroreflex transfer function is inappropriate for system identification of the neural arc but is partially appropriate for the peripheral arc under resting condition, compared with the open-loop analysis. These findings may have great impact, because the closed-loop-spontaneous baroreflex transfer function has been believed to represent the neural arc function (Orea *et al.* 2007; Cooke *et al.* 2009; Ogoh *et al.* 2009).

Methods

Animal preparation

Animals were cared for in strict accordance with the Guiding Principles for the Care and Use of Animals in the Field of Physiological Science approved by the Physiological Society of Japan and the National Cerebral and Cardiovascular Center Research Institute, and the ethical regulations and policies of *The Journal of Physiology* (Drummond, 2009). Ten Japanese white rabbits weighing 2.4–3.3 kg were initially anaesthetized by intravenous injection (2 ml kg^{-1}) of a mixture of urethane (250 mg ml^{-1}) and α-chloralose (40 mg ml^{-1}). Anaesthesia was maintained by continuously infusing the anaesthetics at a rate of 0.33 ml kg^{-1} h^{-1} using a syringe pump (CFV-3200, Nihon Kohden, Tokyo). The rabbits

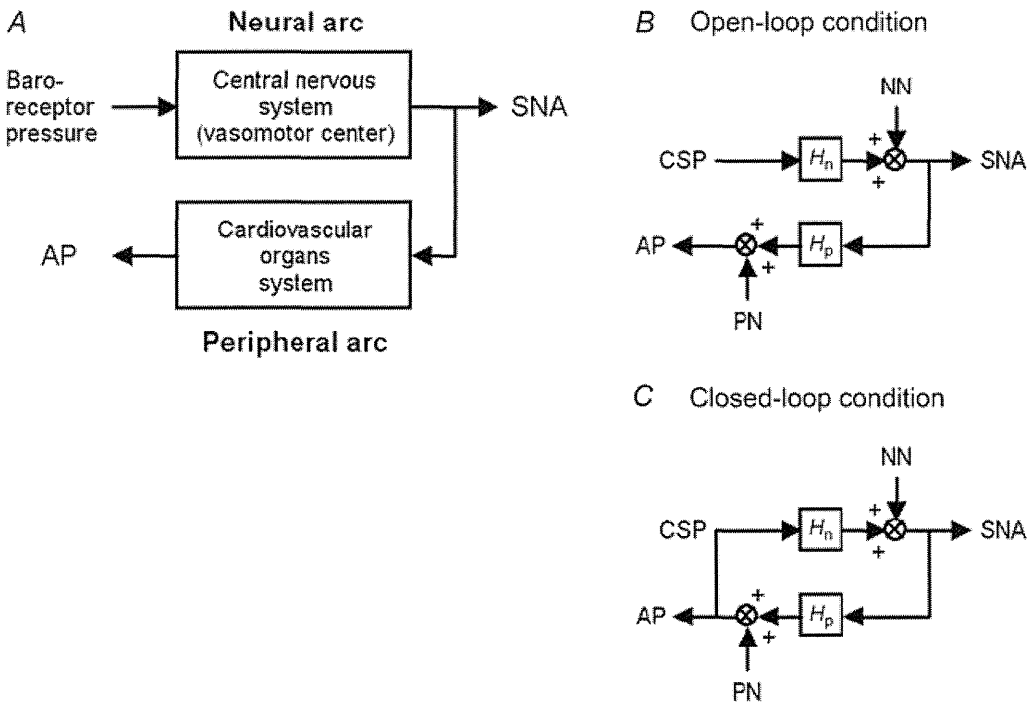

Figure 1. Functional structure of arterial baroreflex system
A, theoretical considerations of the coupling of baroreflex neural and peripheral arcs. Although baroreflex is a negative feedback control system that senses AP by baroreceptors and regulates AP, we opened the loop by changing baroreceptor pressure independent of AP. By measuring SNA, we divided the baroreflex system into the neural arc (from baroreceptor pressure input to efferent SNA via central nervous system) and the peripheral arc (from SNA input to AP via cardiovascular organs system). *B*, block diagram of open-loop baroreflex system. Because of vascular isolation of carotid-sinus regions, CSP is independent of systemic AP. Noise is introduced to the neural and/or peripheral arcs. *C*, block diagram of closed-loop-spontaneous baroreflex system, where CSP equals AP. Noise is introduced to the neural and/or peripheral arcs. Because of the closed-loop nature, changes in AP (and thus, in CSP) control SNA via neural arc transfer function (H_n), which in turn modulate AP via peripheral arc transfer function (H_p). CSP, carotid sinus pressure; SNA, sympathetic nerve activity; AP, arterial pressure; NN, unknown noise in the neural arc; PN, unknown noise in the peripheral arc.

were mechanically ventilated with oxygen-enriched room air. Bilateral carotid sinuses were isolated vascularly from the systemic circulation by ligating the internal and external carotid arteries and other small branches originating from the carotid sinus regions. The isolated carotid sinuses were filled with warmed physiological saline pre-equilibrated with atmospheric air, through catheters inserted via the common carotid arteries. CSP was controlled by a servo-controlled piston pump (model ET-126A, Labworks; Costa Mesa, CA, USA). Bilateral vagal and aortic depressor nerves were sectioned in the middle of the neck region to eliminate reflexes from the cardiopulmonary region and the aortic arch. Systemic AP was measured using a high-fidelity pressure transducer (Millar Instruments; Houston, TX, USA) inserted retrograde from the right common carotid artery below the isolated carotid sinus region. A catheter was inserted into the right femoral vein to infuse phenylephrine and nitroprusside. Body temperature was maintained at around 38°C with a heating pad.

The left renal sympathetic nerve was exposed retroperitoneally. A pair of stainless steel wire electrodes (Bioflex wire AS633, Cooner Wire) was attached to the nerve to record renal SNA. The nerve fibres peripheral to the electrodes were ligated tightly and crushed to eliminate afferent signals. The nerve and electrodes were covered with a mixture of silicone gel (Silicon Low Viscosity, KWIK-SIL, World Precision Instrument, Inc., FL, USA) to insulate and immobilize the electrodes. The pre-amplified SNA signal was band-pass filtered at 150–1000 Hz. These nerve signals were full-wave rectified and low-pass filtered with a cut-off frequency of 30 Hz to quantify the nerve activity.

Protocols

After the surgical preparation, all animals ($n = 10$) were maintained supine. The overall scheme of the experimental design is shown in Fig. 2. Protocols 1–4 were conducted in randomized order at intervals of at least 5 min, while protocol 5 was done finally. In all protocols, bilateral CSP was controlled by a servo-controlled piston pump (Kawada *et al.* 2002). The SNA, CSP and AP were recorded at a sampling rate of 200 Hz using a 12-bit analog-to-digital converter. Data were stored on the hard disk of a dedicated laboratory computer system.

Before these protocols, operating AP and SNA in baroreflex closed-loop condition were determined. First, CSP was matched with systemic AP to close the baroreflex loop. After at least 5 min of stabilization, the variables were recorded for 10 min, and the average AP over 10 min was defined as the operating AP under closed-loop condition.

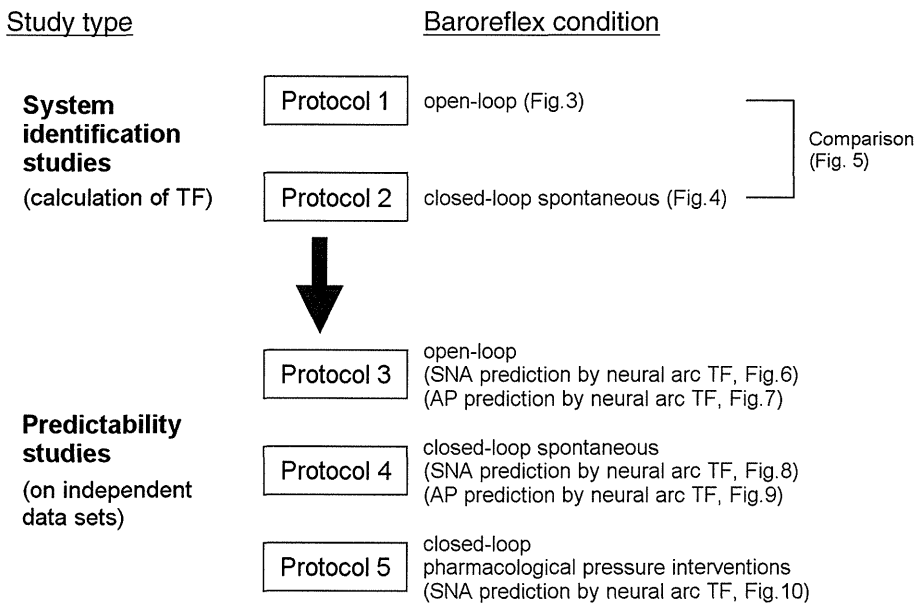

Figure 2. Experimental design
In system identification studies, open-loop (protocol 1, CSP was perturbed according to a binary random sequence) and closed-loop-spontaneous (protocol 2, CSP was matched with systemic AP) baroreflex transfer functions were identified from experimental data. In predictability studies, the predictive power of the above transfer functions was tested using independent data (protocols 3, 4 and 5). Protocol 3 and 4 were open-loop and closed-loop-spontaneous baroreflex conditions, respectively. Protocol 5 was pharmacological pressure intervention by phenylephrine and nitroprusside infusions in closed-loop condition. TF, transfer function; CSP, carotid sinus pressure; SNA, sympathetic nerve activity; AP, arterial pressure.

System identification studies. Protocol 1 was performed to identify the open-loop baroreflex transfer functions. After at least 5 min of stabilization, CSP was randomly assigned at 20 mmHg above or below the operating AP every 500 ms according to a binary random (white-noise) sequence, in which the input power spectrum of CSP was reasonably flat up to 1 Hz (Kawada *et al.* 2002). The variables were recorded for 10 min and stored for analysis.

Protocol 2 was performed to determine the closed-loop-spontaneous baroreflex transfer functions by a convenient method of applying the same calculation as that used in the open-loop condition of protocol 1 (see Appendix A). CSP was matched with systemic AP to close the baroreflex loop. After at least 5 min of stabilization, the variables were recorded for 10 min and stored for analysis.

Predictability studies. Protocols 3, 4 and 5 were performed to investigate the predictability of baroreflex transfer functions. In protocol 3 (open-loop), CSP was randomly assigned at 20 mmHg above or below the operating AP. The variables were recorded for 10 min and stored for analysis.

In protocol 4 (closed-loop), CSP was matched with systemic AP to close the baroreflex loop. After at least 5 min of stabilization, the variables were recorded for at least 10 min and stored for analysis.

Protocol 5 was also performed to investigate the predictability of baroreflex transfer functions during sequential pharmacological pressure interventions in the closed-loop condition. CSP was matched with systemic AP. After at least 2 min of stabilization, phenylephrine hydrochloride (3 μg kg^{-1}) was bolus infused through a venous catheter inserted into the right femoral vein, followed 1–2 min later by sodium nitroprusside (4 μg kg^{-1}) and then 1–2 min later by the second phenylephrine hydrochloride infusion (4 μg kg^{-1}). The variables were recorded continuously for at least 10–11 min and stored for analysis.

Data analysis

SNA signal was normalized by the following steps. First, 0 arbitrary unit (a.u.) was assigned to the post-mortem noise level. Second, 100 a.u. was assigned to the SNA signals averaged over 10 min before protocols. Last, the other SNA signals in protocols 1–5 were then normalized to these values.

In protocol 1, we calculated the open-loop transfer (gain and phase) and coherence functions from CSP input to SNA in the neural arc ($H_{\text{n-open}}$) and from SNA to AP in the peripheral arc ($H_{\text{p-open}}$). We re-sampled CSP and SNA at 10 Hz and segmented them into 10 sets of 50% overlapping bins of 2^{10} data point each. The segment length was 102.4 s, which yielded the lowest frequency bound of 0.01 (0.0097) Hz. We subtracted a linear trend and applied a Hanning window for each segment. We then performed fast Fourier transform to obtain frequency spectra of input (x) and output (y). The inputs are CSP and SNA, while the outputs are SNA and AP in the neural and peripheral arc subsystems, respectively. We ensemble averaged the input power ($Sxx(f)$), output power ($Syy(f)$), and cross power between input and output ($Syx(f)$) over the 10 segments. Then, we calculated the transfer function ($H(f)$) from input to output as follows:

$$H(f) = \frac{Syx(f)}{Sxx(f)} \tag{1}$$

Although individual noise may be present in the neural and peripheral arc subsystems, the effects of noise on the calculations of transfer functions are eliminated by open-loop operation and white-noise-like perturbation of CSP (see Appendix A, Fig. 1*A*).

To quantify the linear dependence between input and output in the frequency domain, we calculated the magnitude-squared coherence function (Coh(f)) as follows:

$$\text{Coh}(f) = \frac{|Syx(f)|^2}{Sxx(f)Syy(f)} \tag{2}$$

The coherence values range from zero to unity. Unity coherence indicates a perfect linear dependence between input and output, whereas zero coherence indicates total independence of these two signals. To quantify the errors on individual gain and phase estimates, we calculated the normalized random error ($\varepsilon(f)$) as follows:

$$\varepsilon(f) = \sqrt{\frac{1 - \text{Coh}(f)}{2n_{\text{d}}\text{Coh}(f)}} \tag{3}$$

where n_{d} is the number of distinct subrecord, when the error in gain factor estimate matches that in phase factor estimate (Julius & Allan, 2000).

To quantify the transfer characteristics in the time domain, step response was calculated by discrete from convolution integral as follows:

$$Y(t) = \sum_{\tau=0}^{N} h(\tau) \cdot X(t-\tau) \tag{4}$$

where $h(\tau)$ is the impulse response obtained by inverse fast Fourier transform of the transfer function ($H(f)$); N is the total number of data elements; τ is the convolution parameter; t is time in increments of 0.1 s (or 10 Hz); $X(t) = 0$ for $t < 0$ and $X(t) = 1$ for $t \geq 0$.

It should be noted that since protocol 2 was a closed-loop and spontaneous baroreflex condition, unknown noise, if present in the neural and peripheral arc subsystems, would affect the accuracy of system identification (see Appendix A, Fig. 1*B*). Based on earlier

studies (Cooke *et al.* 1999, 2009; Ogoh *et al.* 2009), we applied a simplified (open-loop-like) calculation of transfer function to the closed-loop-spontaneous resting baroreflex condition, and estimated the closed-loop-spontaneous baroreflex transfer functions from AP input to SNA in the neural arc ($H_{\text{n-closed-spon}}$) and from SNA to AP in the peripheral arc ($H_{\text{p-closed-spon}}$), together with coherence functions and step responses (see Appendix A).

In protocols 3 and 4, we calculated the predicted time-series output dynamics (SNA and AP) from measured input signals (CSP/AP and SNA in the neural and peripheral arc, respectively), using eqn (4) and impulse response obtained from the transfer functions in protocols 1 and 2. The predicted output was scatter-plotted, and compared with the actually measured output by calculating the linear correlation coefficient (r) and root mean square (RMS). The analysis was performed using the data at arbitrarily selected 1 and 3 min in protocols 3 and 4, respectively.

In protocol 5, similar to protocol 3 and 4, we calculated the predicted time-series output dynamics of SNA from measured pressure input signals (CSP/AP in the neural arc) during pharmacological interventions. The predicted SNA was scatter-plotted, and compared with the actual SNA measurements by calculating r and RMS. The analysis was performed using the data for 10–11 min. Since AP was determined by interventions (phenylephrine and nitroprusside infusions) and not by SNA, we did not calculate the predicted AP dynamics from the measured SNA signals.

Statistic analysis

All data are presented as means ± SD. Paired t test and repeated measures analysis of variance with *post hoc* multiple comparisons were used to compare variables as appropriate. Differences were considered significant when $P < 0.05$.

Results

Open-loop transfer function (protocol 2)

Figure 3 shows a typical example of the open-loop system identification of baroreflex transfer functions in protocol 2. CSP was perturbed according to a binary random (white-noise) sequence at 500 ms intervals (Fig. 3*A*, green line). When CSP was increased, SNA decreased, and vice versa. In the frequency domain, the input power spectrum of CSP was reasonably flat up to 1 Hz (Fig. 3*B*, green line).

The open-loop transfer function of the neural arc from CSP input to SNA ($H_{\text{n-open}}$; Fig. 3*C*, left panels) showed that the gain increased as the frequency of CSP perturbation increased between 0.01 Hz and 0.4 Hz, indicating dynamic high-pass characteristics. The phase approached $-\pi$ at the lowest frequency, indicating a negative SNA response to CSP changes, and lagged as the frequency increased (Fig. 3*C*, left panels). The coherence was over 0.8 between 0.03 to 0.4 Hz except at around 0.35 Hz (Fig. 3*C*, left panels). The step response (Fig. 3*D*, left panel) of SNA in response to CSP consisted of an initial decrease followed by partial recovery and then steady state.

The open-loop transfer function of the peripheral arc from SNA input to AP ($H_{\text{p-open}}$, Fig. 3*C*, right panels) showed that the gain decreased as the frequency increased, indicating low-pass characteristics. The phase approached zero at the lowest frequency, indicating a positive AP response to SNA changes, and lagged as the frequency increased. The coherence was over 0.8 between 0.01 to 0.3 Hz except at around 0.2 Hz (Fig. 3*C*, right panels). The step response (Fig. 3*D*, right panel) of SNA to CSP was a gradual increase to steady state.

The transfer function of baroreflex total arc from CSP input to systemic AP identified in the open-loop condition (Fig. 3*E*) showed that the gain decreased as the frequency increased, indicating low-pass characteristics that were milder than $H_{\text{p-open}}$. The phase approached $-\pi$ at the lowest frequency, indicating negative feedback system characteristics of baroreflex (negative AP response to CSP changes). The phase lagged as frequency increased. The transfer function of total arc was almost consistent with multiplication of tandemly arranged open-loop transfer functions of neural ($H_{\text{n-open}}$) and peripheral ($H_{\text{p-open}}$) arcs (Fig. 1*A* and *B*), at the frequency where their coherence functions were high.

Closed-loop-spontaneous transfer function (protocol 3)

Figure 4 shows a typical example of the closed-loop-spontaneous transfer functions simplified, calculated in protocol 3 by applying open-loop-like calculations to closed-loop-spontaneous data. The data were obtained from the same animal as in Fig. 3.

We closed the baroreflex loop by matching CSP with systemic AP. The exact match of the two parameters was demonstrated by autospectrum (Fig. 4*B*) and beat-to-beat waveform (Fig. 4*C*), both showing overlapping of CSP (green line) and systemic AP (black line). The exact match was further confirmed by the transfer functions from CSP to systemic AP (Fig. 4*D*), which showed that the gain, phase and coherence functions were maintained constant at 1, zero and 1, respectively.

The closed-loop-spontaneous transfer function of the neural arc ($H_{\text{n-closed-spon}}$) from CSP (that equalled AP) to SNA (Fig. 4*E*, left panels, black line) was markedly different from the open-loop transfer function ($H_{\text{n-open}}$, red line) with respect to gain, phase, coherence and step response. The increase in gain *versus* frequency was

steeper; the gain was thus higher and the coherence was lower in $H_{\text{n-closed-spon}}$ compared with $H_{\text{n-open}}$. The phase led as frequency increased, while the step response oscillated (Fig. 4*F*, left panel) in $H_{\text{n-closed-spon}}$, which were markedly different from $H_{\text{n-open}}$.

In contrast to the neural arc, the closed-loop-spontaneous transfer function for the peripheral arc ($H_{\text{p-closed-spon}}$) from SNA to AP (Fig. 4*E*, right panels, black line) approximated that of the open-loop transfer function ($H_{\text{p-open}}$, red line). The gain (except at 0.02–0.05 Hz) and phase were similar up to 0.3 Hz, although the coherence was lower in $H_{\text{p-closed-spon}}$ than in $H_{\text{p-open}}$ (common feature for both neural and peripheral arcs). The step response was similar to that of $H_{\text{p-open}}$ except for a slower time constant (Fig. 4*F*, right panel). Because of the closed-loop condition, the gain and phase functions of $H_{\text{p-closed-spon}}$ were the inverse of those of $H_{\text{n-closed-spon}}$.

Since CSP exactly matched systemic AP in this closed-loop-spontaneous baroreflex condition, the transfer function of total arc baroreflex from CSP input to systemic AP was calculated as all-pass filter without modulating phase (Fig. 4*D*). This is greatly different from the transfer function of the total arc identified from open-loop experiments (Fig. 3*E*).

Comparison between open-loop and closed-loop-spontaneous transfer functions

The closed-loop-spontaneous transfer functions (Fig. 5*A*, blue lines) ($H_{\text{n-closed-spon}}$ and $H_{\text{p-closed-spon}}$) obtained from

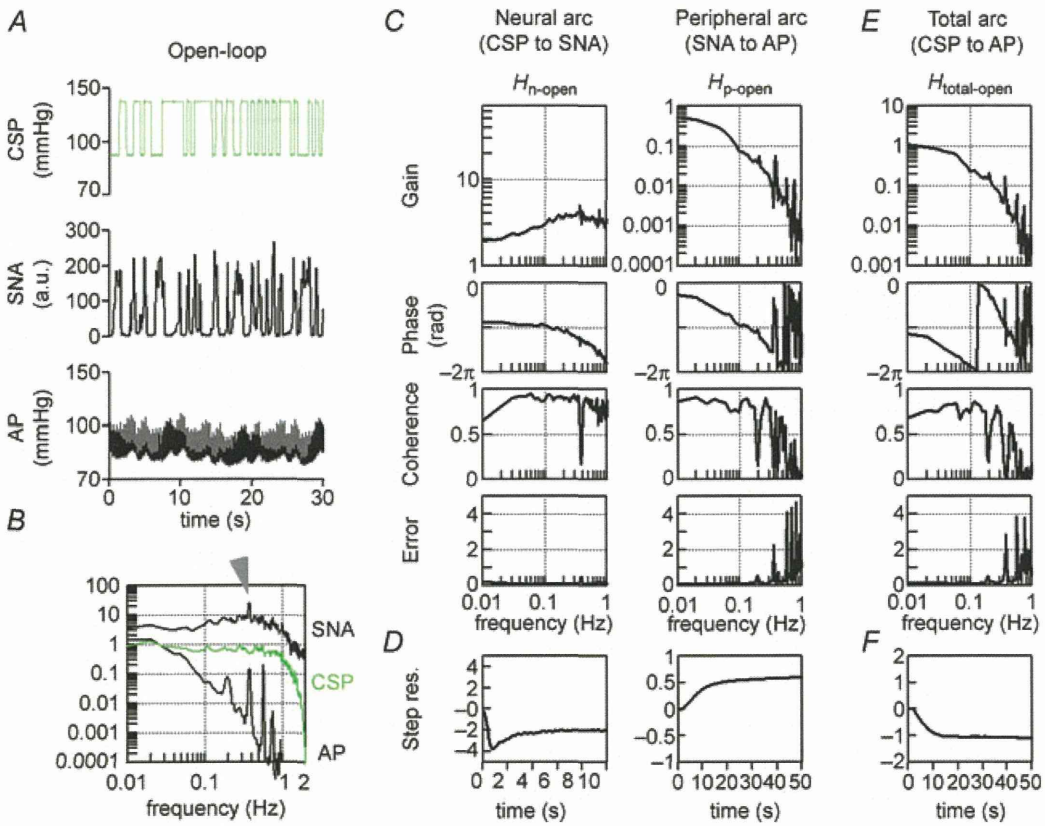

Figure 3. Open-loop transfer function
A, typical representative data of one rabbit in protocol 2, showing time series of carotid sinus pressure (CSP), sympathetic nerve activity (SNA) and systemic arterial pressure (AP) during CSP perturbation in open-loop baroreflex condition. CSP is changed according to a binary random (white-noise) signal with a switching interval of 500 ms. *B*, input power spectrum of CSP (green line) is reasonably flat up to 1 Hz. Autospectra of SNA (top line) and systemic AP (bottom line) are also shown. The arrowhead indicates a peak of SNA autospectrum at 0.4 Hz. *C*, open-loop transfer functions of the neural arc ($H_{\text{n-open}}$) from CSP input to SNA (left panels) and of the peripheral arc ($H_{\text{p-open}}$) from SNA input to AP (right panels) identified in the same animal as in A. The gain (top), phase (second), coherence (third) and normalized random error (Error, bottom) functions are shown. Units of gain are [a.u. mmHg^{-1}] for the neural arc and [mmHg a.u.$^{-1}$] for the peripheral arc, respectively. *D*, step responses (Step res.) derived from the transfer functions shown in *C*. The units are [a.u.] for the neural arc and [mmHg] for the peripheral arc, respectively. *E*, open-loop transfer functions of the total arc ($H_{\text{total-open}}$) from CSP input to AP identified in the same animal as in A. The gain (top), phase (second), coherence (third) and normalized random error (Error, bottom) functions are shown. Unit of gain is [mmHg mmHg^{-1}]. *F*, step response (Step res.) derived from the transfer function shown in *E*. The unit is [mmHg]. a.u., arbitrary unit.

all animals ($n = 10$) in protocol 2 were compared with the open-loop transfer functions (Fig. 5*A*, red lines) in protocol 1. The step response was also compared between closed-loop-spontaneous (Fig. 5*B*, blue line) and open-loop experiments (Fig. 5*B*, red line).

In the neural arc (Fig. 5*A* and *B*, left panels; Table 1), closed-loop-spontaneous transfer functions ($H_{\text{n-closed-spon}}$, blue lines) were markedly different from open-loop transfer functions ($H_{\text{n-open}}$, red lines), similar to the example shown in Fig. 4*E*. The difference was characterized by an enhanced increase of gain *versus* frequency (slope), a phase lead and an oscillation of step response. In contrast, in the peripheral arc (Fig. 5*A* and *B*, right panels; Table 2), closed-loop-spontaneous transfer functions ($H_{\text{p-closed-spon}}$) were similar to open-loop transfer functions ($H_{\text{n-open}}$) in gain, phase and step response.

The transfer function of the baroreflex total arc from CSP input to systemic AP in the open-loop condition was identified as having low-pass filter characteristics with negative feedback in all animals. In contrast, the total arc transfer function in the closed-loop-spontaneous condition had all-pass filter characteristics without modulating phase in all animals.

Predictability of open-loop and closed-loop-spontaneous transfer function compared with data measured in open-loop condition (protocol 3)

The ability of the neural arc transfer functions (determined by protocols 1 and 2) to predict output dynamics (SNA) from given input signals (CSP) in the open-loop

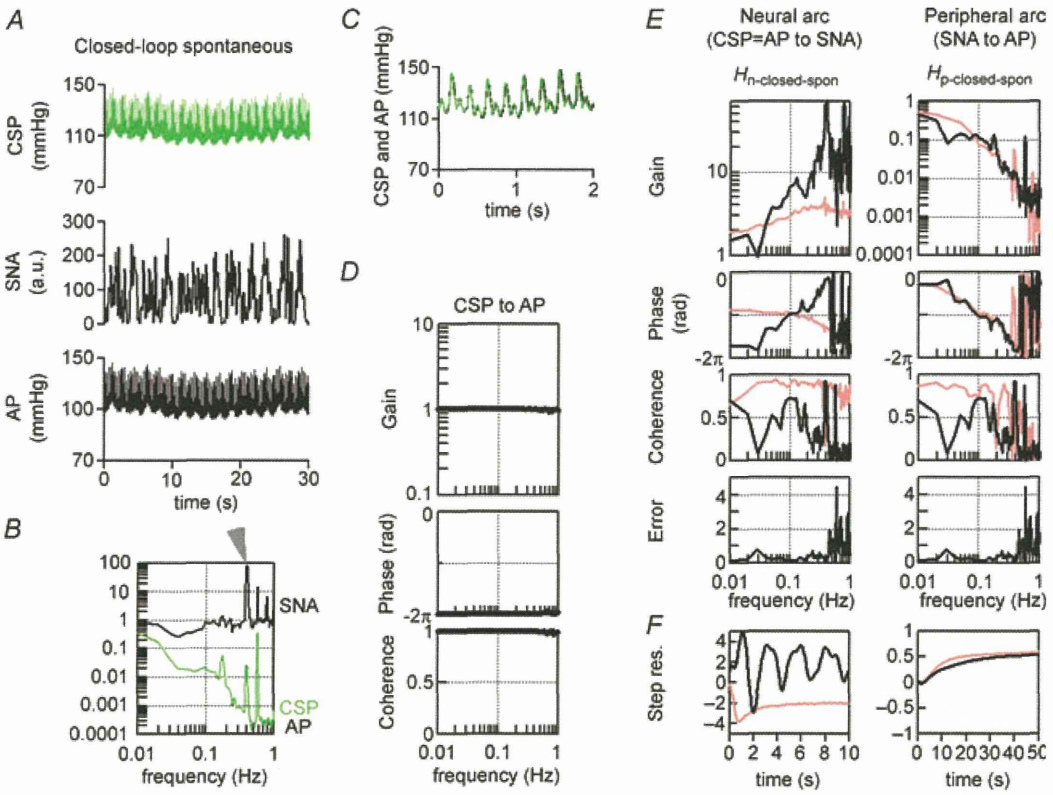

Figure 4. Closed-loop-spontaneous transfer function
A, typical representative data of protocol 3, showing time series of CSP, SNA and systemic AP in closed-loop-spontaneous baroreflex condition, where CSP is matched with systemic AP. The data were obtained from the same animal as in Figure 3. *B–D* show exactness of good match between CSP and systemic AP. *B*, auto-spectrum of CSP (green line) overlaps with that of AP (black line). Autospectrum of SNA (top line) is also shown. The arrowhead indicates a peak in the SNA autospectrum at 0.4 Hz. *C*, beat-to-beat waveform of CSP (green line) overlaps with that of AP (black line). *D*, the transfer functions from CSP to systemic AP. Gain (top), phase (middle) and coherence (bottom) functions are shown. Unit of gain is [mmHg mmHg^{-1}]. *E*, the closed-loop-spontaneous transfer functions of the neural arc ($H_{\text{n-closed-spon}}$) from CSP (=AP) input to SNA (left panels) and of the peripheral arc ($H_{\text{p-closed-spon}}$) from SNA input to AP (right panels) identified in the same animal as in *A*. The gain (top), phase (second), coherence (third) and normalized random error (bottom) functions are shown. Units of gain are [a.u. mmHg^{-1}] for the neural arc and [mmHg a.u.$^{-1}$] for the peripheral arc, respectively. *F*, step responses (Step res.) derived from the transfer functions. The units are [a.u.] for the neural arc and [mmHg] for the peripheral arc, respectively. a.u., arbitrary unit; CSP, carotid sinus pressure; SNA, sympathetic nerve activity; AP, arterial pressure; Step res., step response. In *E* and *F*, the open-loop transfer functions and derived step responses are included for reference (red lines).

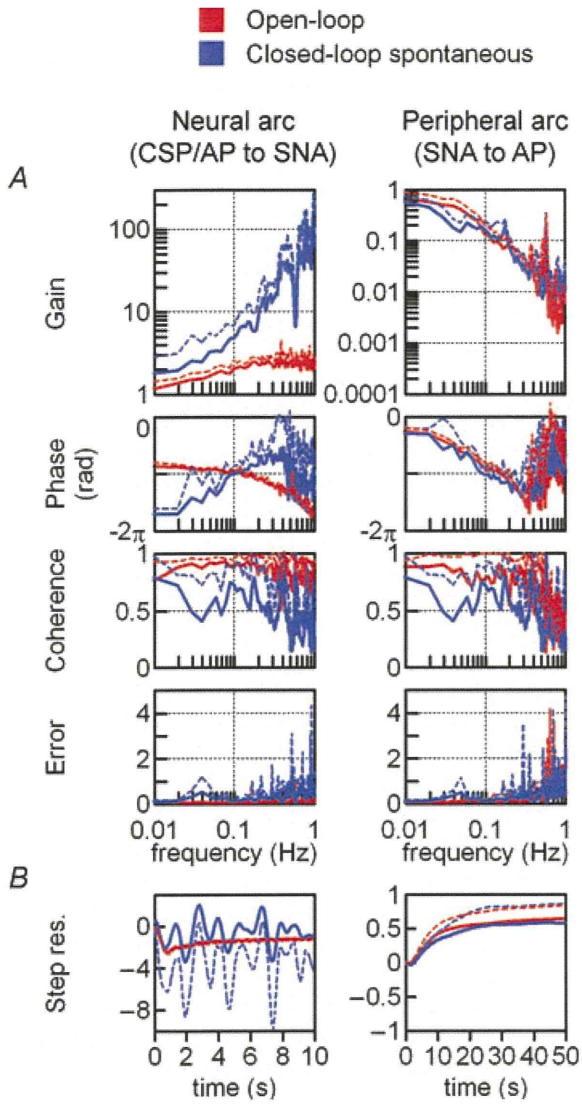

Figure 5. Comparison between open-loop and closed-loop-spontaneous transfer functions
Solid and dashed lines represent the mean and mean + SD, respectively, obtained from all animals (n = 10). *A*, red lines are open-loop transfer functions of the neural ($H_{n\text{-}open}$, left panels) and peripheral arcs ($H_{p\text{-}open}$, right panels) identified in protocol 1. Blue lines are closed-loop-spontaneous transfer functions (blue lines) of the neural ($H_{n\text{-}closed\text{-}spon}$, left panels) and peripheral arcs ($H_{p\text{-}closed\text{-}spon}$, right panels) identified in protocol 2. The gain (top), phase (second), coherence (third) and normalized random error (bottom) functions are shown. Units of gain are [a.u. $mmHg^{-1}$] for the neural arc and [mmHg $a.u.^{-1}$] for the peripheral arc, respectively. The closed-loop-spontaneous baroreflex transfer function for the neural arc is markedly different from the open-loop transfer function, whereas that for the peripheral arc partially matches the open-loop transfer function. *B*, step response (Step res.) calculated from the open-loop (red lines) and closed-loop-spontaneous (blue lines) transfer functions. The units are [a.u.] for the neural arc and [mmHg] for the peripheral arc, respectively. a.u., arbitrary unit; CSP, carotid sinus pressure; SNA, sympathetic nerve activity; AP, arterial pressure; Step res., step response.

Table 1. Transfer functions of the baroreflex neural arc (from CSP to SNA) in open-loop and closed-loop-spontaneous conditions

	Open-loop TF ($H_{n\text{-}open}$, CSP to SNA)	Closed-loop-spontaneous TF ($H_{n\text{-}closed\text{-}spon}$, CSP [= AP] to SNA)
Gain (a.u. $mmHg^{-1}$)		
0.01 Hz	1.2 ± 0.2	1.8 ± 0.1*
0.1 Hz	2.0 ± 0.3	5.3 ± 2.8*
0.3 Hz	2.6 ± 0.3	14.6 ± 5.7*
Phase (rad)		
0.01 Hz	−2.7 ± 0.2	−5.4 ± 0.4*
0.1 Hz	−3.0 ± 0.1	−3.1 ± 0.4
0.3 Hz	−3.7 ± 0.1	−2.6 ± 0.11*
Coherence		
0.01 Hz	0.8 ± 0.1	0.8 ± 0.2
0.1 Hz	0.9 ± 0.1	0.6 ± 0.2*
0.3 Hz	0.9 ± 0.1	0.4 ± 0.3*
Slope (dB per decade)		
0.01 Hz to 0.3 Hz	4.7 ± 0.4	12.1 ± 6.1*
Step response		
Initial response (a.u.)	−2.4 ± 0.2	Oscillating response
Steady-state level (a.u.)	−1.2 ± 0.2	

Values are mean ± SD ($n = 10$). *$P < 0.05$; open-loop *vs.* closed-loop-spontaneous conditions. TF, transfer function.

Table 2. Transfer functions of baroreflex peripheral arc (from SNA to AP) in open-loop and closed-loop-spontaneous conditions

	Open-loop TF ($H_{p\text{-}open}$, SNA to AP)	Closed-loop-spontaneous TF ($H_{p\text{-}closed\text{-}spon}$, SNA to AP)
Gain (mmHg $a.u.^{-1}$)		
0.01 Hz	0.7 ± 0.2	0.6 ± 0.2
0.1 Hz	0.1 ± 0.1	0.1 ± 0.1
0.3 Hz	0.03 ± 0.01	0.03 ± 0.02
Phase (rad)		
0.01 Hz	−0.8 ± 0.2	−0.9 ± 0.2
0.1 Hz	−3.0 ± 0.2	−3.0 ± 0.2
0.3 Hz	−4.2 ± 0.1	−4.0 ± 0.3
Coherence		
0.01 Hz	0.9 ± 0.1	0.8 ± 0.2
0.1 Hz	0.8 ± 0.2	0.6 ± 0.2*
0.3 Hz	0.9 ± 0.1	0.4 ± 0.3*
Step response		
Steady-state level (mmHg)	−0.7 ± 0.2	−0.6 ± 0.2

Values are mean ± SD ($n = 10$). *$P < 0.05$; open-loop *vs.* closed-loop-spontaneous conditions. TF, transfer function.

condition was quantified by comparing with the actual measurements of SNA response to CSP changes in protocol 3. Figure 6 shows a typical example obtained from the same animal as in Figs 1 and 2. CSP was randomly